Alexandria Engineering Journal 80 (2023) 167–190

Contents lists available at ScienceDirect

Alexandria Engineering Journal

journal homepage: www.elsevier.com/locate/aej

Original Article

Modelling the impacts of media campaign and double dose vaccination in controlling COVID-19 in Nigeria

N.I. Akinwande [a], S.A. Somma [d], R.O. Olayiwola [a], T.T. Ashezua [d], R.I. Gweryina [d,*], F.A. Oguntolu [a], O.N. Abdurahman [a], F.S. Kaduna [d], T.P. Adajime [e], F.A. Kuta [b], S. Abdulrahman [f], A.I. Enagi [a], G.A. Bolarin [a], M.D. Shehu [a], A. Usman [c]

[a] Department of Mathematics, Federal University of Technology Minna, Nigeria
[b] Department of Microbiology, Federal University of Technology Minna, Nigeria
[c] Department of Statistics, Federal University of Technology Minna, Nigeria
[d] Department of Mathematics, Federal University of Agriculture, Makurdi, Nigeria
[e] Department of Epidemiology and Community Health, Benue State University, Makurdi, Nigeria
[f] Department of Mathematics, Federal University Birnin Kebbi, Nigeria

ARTICLE INFO

Keywords:
COVID-19
Media campaign
Double-dose vaccination
Stability
Bifurcation
Optimal control

ABSTRACT

Corona virus disease (COVID-19) is a lethal disease that poses public health challenge in both developed and developing countries of the world. Owing to the recent ongoing clinical use of COVID-19 vaccines and non-compliance to COVID-19 health protocols, this study presents a deterministic model with an optimal control problem for assessing the community-level impact of media campaign and double-dose vaccination on the transmission and control of COVID-19. Detailed analysis of the model shows that, using the Lyapunov function theory and the theory of centre manifold, the dynamics of the model is determined essentially by the control reproduction number (R_{mv}). Consequently, the model undergoes the phenomenon of forward bifurcation in the absence of the double dose vaccination effects, where the global disease-free equilibrium is obtained whenever $R_{mv} \leq 1$. Numerical simulations of the model using data relevant to the transmission dynamics of the disease in Nigeria, show that, certain values of the basic reproduction number (($R_0 \geq 7$)) may not prevent the spread of the pandemic even if 100% media compliance is achieved. Nevertheless, with assumed 75% (at $R_0 = 4$)) media efficacy of double dose vaccination, the community herd immunity to the disease can be attained. Furthermore, Pontryagin's maximum principle was used for the analysis of the optimized model by which necessary conditions for optimal controls were obtained. In addition, the optimal simulation results reveal that, for situations where the cost of implementing the controls (media campaign and double dose vaccination) considered in this study is low, allocating resources to media campaign-only strategy is more effective than allocating them to a first-dose vaccination strategy. More so, as expected, the combined media campaign-double dose vaccination strategy yields a higher population-level impact than the media campaign-only strategy, double-dose vaccination strategy or media campaign-first dose vaccination strategy.

1. Introduction

The emergence of COVID-19 in December 2019 (in China) has brought remarkable disruption with wider socio-economic implications globally. The spread of the virus has cut across many countries of the world with morbidity and mortality estimated to be over 581.8 million and 6.4 million

* Corresponding author.
E-mail addresses: ninuola.wande@futminna.edu.ng (N.I. Akinwande), sam.abu@futminna.edu.ng (S.A. Somma), olayiwola.rasaq@futminna.edu.ng (R.O. Olayiwola), ttashezua@gmail.com (T.T. Ashezua), gweryina.reuben@uam.edu.ng (R.I. Gweryina), festus.tolu@futminna.edu.ng (F.A. Oguntolu), nurat.a@futminna.edu.ng (O.N. Abdurahman), kadunafrancis@gmail.com (F.S. Kaduna), tadajime@bsum.edu.ng (T.P. Adajime), farukkuta@gmail.com (F.A. Kuta), sirajo.enagi@gmail.com (S. Abdulrahman), enagi.idris@futminna.edu.ng (A.I. Enagi), g.bolarin@futminna.edu.ng (G.A. Bolarin), m.shehu@futminna.edu.ng (M.D. Shehu), abu.usman@futminna.edu.ng (A. Usman).

https://doi.org/10.1016/j.aej.2023.08.053
Received 1 March 2023; Received in revised form 27 July 2023; Accepted 16 August 2023
Available online 25 August 2023

cases respectively as at 7th August, 2022 according to the World Health Organization (WHO) [1]. On February 27, 2020, the first case of COVID-19 was confirmed in Nigeria when an Italian national was tested positive of the virus in Lagos as reported by the Federal Ministry of Health (FMOH) [2]. After the index case, most states in Nigeria became vulnerable to the virus and as at 12th August, 2022, over 262,402 cases and 3,147 deaths have been confirmed as reported by the Nigeria Centre for Disease Control (NCDC) [3].

Worldwide, health campaigns via social media and other awareness platforms have proven to be an effective non-pharmaceutical intervention in controlling infectious diseases. At the beginning of an epidemic when medical healthcare facilities and vaccination are inadequate to curb the disease burden, one can reliably adopt media as the partial treatment strategy with no cost consequences. Till date, media is the main source of information with noticeable impact on individual's behaviour towards the outbreak of a disease. It is the vehicle through which people become aware, get educated about the disease and take precautionary measures such as vaccination, social distancing, quarantine and wearing protective masks to reduce the probability of being infected [4,5]. Therefore, as recommended by Khajanchi et al. [5], implementing media campaign with double dose vaccination in curtailing COVID-19 could be a welcome development.

In all the preventive measures mentioned above, double dose vaccination as a standard prevention strategy for COVID-19 has not been given full compliance in Nigeria. Since COVID-19 vaccination began in Nigeria on March 5, 2021, only 8 million out of 18 million vaccinated people (an approximate) have received the second dose of COVID-19 vaccine as documented by the National Primary Health Care Development Agency (NPCDA) [6]. Due to the non-compliance of COVID-19 health protocols in recent times and the fact that first dose of COVID-19 vaccine alone has no capacity to fully confer immunity to the population [7], it became imperative to examine the impacts of media campaign and the administration of first and second doses of COVID-19 vaccine on the transmission dynamics of the disease.

Mathematical modelling has been a veritable tool in providing insights into the transmission dynamics, prevention and control of infectious diseases [8,9]. So far many works have been done on COVID-19, but for lack of space we will restrict our review to the most recent and relevant papers. In 2020, Zeb et al. [10] carried out a mathematical research on the control of COVID-19 using isolation strategy on the infected population. Findings from their study revealed that the method can reduce the probability for the future spread of the pandemic. Maji et al. [11] developed a delay model for COVID-19 with a view to assessing the impact of awareness-based control measures on the transmission dynamics of the disease. Samui et al. [12] developed a mathematical model to study the reported and unreported cases of COVID-19 in India. One among the findings of the study predicted a higher peak of the disease after 60 days and the disease continue to persist for a long time. However, the presence of vaccination will remarkably change the outcome. In another study, Sitthiwirattham et al. [13] constructed a discrete mathematical model for COVID-19 in order to explore in real life the transmission structures of the disease with special reference to COVID-19 outbreaks in India and Algeria. The study by Alqudah et al. [14] examined the effect of weather conditions on the spread of COVID-19 using Eigenspace Decomposition Approach. The technique has shown that wind speed has the major effect on rapid spread of the disease. Furthermore, several authors have studied the spread and control of corona virus using stochastic modelling approach [15–17].

In another development, [18–22] formulated fractional order mathematical models for COVID-19 without double dose vaccination. However, Zhang et al. [18] introduced isolation class into their model, Zeb et al. [21,22] accounts for the role of quarantine and vaccination (with no special reference to the levels of vaccination) while Bushnaq et al. [19] conducted mathematical assessment of media education and quarantine on the spread of corona virus. The work of Tiwari et al. [23] examined the effects of community awareness and global information campaigns on the dynamics of coronavirus; and their study suggested that social media and mouth-mouth awareness if effectively implemented can mitigate the spread of the disease. Despite the robust nature of the findings, the study lacks an in-depth threshold analysis of the basic reproduction number, and the authors further recommended the extension of their model by incorporating vaccination alongside awareness of COVID-19. This is an open problem the present study intend to explore. Rai et al. [24] explored the impact of social media advertisements with quarantine on the spread of COVID-19 pandemic in the presence of asymptomatic, symptomatic and aware individuals. The research findings projected continuous awareness (via social media and internet platforms) and quarantine of asymptomatic individuals to be good candidate strategies for reducing COVID-19 burdens in India. Mondal and Khajanchi [25] formulated an SAIQJR model with optimal control intervention strategies to control the transmission of COVID-19. Sensitivity and numerical results of the study have shown that transmission parameters with the implementation of the three optimal controls are key in reducing the prevalence of the disease. Another study of Khajanchi et al. [5] analyzed a compartmental epidemiological model of SARS-CoV-2 virus with the prediction that the intensity of the epidemic peak will decrease as the control interventions are optimally implemented. Khajanchi et al. [26] carried out a study on the transmission of COVID-19 in India with the effect of hospitalization. The result of their work predicted an oscillatory behaviour of COVID-19 cases in India and further concluded that COVID-19 might become a seasonal disease.

The works of [27–30] formulated COVID-19 models of the first dose vaccination with optimality control. Other modellers of COVID-19 have developed mathematical models that incorporate quarantine and isolation [31], social distancing and treatment [32], use of face masks and hand sanitizers [33] and awareness campaign [34]. The effect of denial on the early spread of COVID-19 was researched by Gweryina et al. [35]. More so, [36,37] conducted studies on model forecasting of COVID-19 cases in India.

Recent studies [38–42] have constructed models of COVID-19 transmission dynamics with double-dose vaccination using bilinear incidence function (or mass action). Though Paul and Kuddus [38] implemented this control strategy in Bangladesh, where the population is assumed constant (birth and death rates are the same), Akuka et al. [39] and Ayoola et al. [40] conducted their studies for varying populations. Peter et al. [41] developed mathematical model of COVID-19 pandemic with the aim of examining the usefulness of double dose vaccination without taking into account the effects of infection outbreak among vaccinated population. On the other hand, Sepulveda et al. [42] carried out analysis of a COVID-19 model involving two vaccination doses with delay effects but the impact of media campaign was not considered.

Motivated by the works of [23,24,38–42], we formulate (in line with our goal) a mathematical model for assessing the impacts of media campaign and double dose vaccination in line with the recommendation in the work of Tiwari et al. [23]. Furthermore, the basic model is extended to an optimal control problem in order to minimize the cost of double vaccination and media campaign. The present study intends to address the following research objectives:

* to study the transmission dynamics of COVID-19 using compartmental modelling;
* to analyze the model using global stability and bifurcation approaches;
* to obtain the minimum threshold value for media campaign coverage on double dose vaccination needed to attain herd immunity for the disease;
* to determine the parameters responsible for the rapid spread of corona virus using normalized forward sensitivity index; and
* to obtain optimal control strategies necessary for the reduction in COVID-19 cases.

The foregoing notwithstanding, the original contributions of this paper to the modelling of COVID-19 are as follows:

(i) incorporating media campaign and double dose vaccination into an optimal control model as recommended by Tiwari et al. [23],
(ii) allowing the outbreak of infection (with standard incidence) among the first-dose vaccinated individuals as supported by Centers for Disease Control and Prevention (CDC) [43].

The justification for using the standard incidence, rather than mass action, stems from the fact that, (i) the number of effective contacts between infective and susceptible individuals may reduce as a result of the preventive measures taken by, and behavioural changes of, susceptible individuals in response to the increasing cases of the disease [44,45], (ii) bilinear incidence function is most useful for the initial epidemic outbreaks, and may not be applicable for large data sets [46] considering the present cases of COVID-19 pandemic globally.

The organization of the paper is as follows: The model is formulated in Section 2. Basic properties of the model are presented in Section 3. The existence and stability of disease-free equilibrium is analyzed in Section 4. In Section 5, the existence and stability of the endemic equilibrium is established. The model formulated in Section 2 is extended to an optimal control problem and analyzed in Section 6. The simulation results of the model were discussed in Section 7. The conclusion containing the main findings of the study is given in Section 8, and model limitations are presented in Section 9.

2. Model formulation

The model for the transmission dynamics of COVID-19, in the presence of media campaign and double dose vaccination, within a population, is formulated by partitioning the total human population, $N(t)$ at time t into nine sub-populations of the susceptibles $S(t)$, vaccinated individuals at stage 1 (first dose) $V_1(t)$, vaccinated individuals at stage 2 (second dose) $V_2(t)$, latently infected $L(t)$, quarantined $Q(t)$, asymptomatic infectious $I_a(t)$, symptomatic infectious $I_s(t)$, hospitalized (isolated) $P(t)$ and recovered $R(t)$ individuals. Note that stages V_1 and V_2 represent the boosting of the vaccine derived efficacy, with those in V_2 class having stronger vaccine protection compared to those in the V_1 class. Susceptible individuals are recruited at a constant rate Λ. $\tau_1\lambda$ is the rate of infection due to the interactions between the susceptible with the asymptomatic and symptomatic individuals while $\tau_2\lambda$ is the outbreak of infection among the vaccinated group after the first dose of COVID-19 vaccine is received at a rate ρ_1. First dose vaccinated individuals on receiving the second dose of vaccination progresses to the second vaccinated class at a rate ρ_2. First dose vaccinated individuals regain susceptibility after the vaccine wanes at a rate ω. Second dose vaccinated individuals are removed at a rate ρ_3. Individuals in latent class are either quarantined at a rate θ or progresses to symptomatic and asymptomatic classes at rate $\sigma\psi$ and $\sigma(1-\psi)$ respectively, where ψ is the proportion of latent individuals that become symptomatic. The individuals in quarantine, asymptomatic and symptomatic classes are hospitalized at the rates ϕ_1, ϕ_2 and ϕ_3 respectively. Asymptomatic individuals show symptoms of the disease at a rate ξ while the latent, and quarantined individuals recover without treatment at the rates γ_1 and γ_2 respectively. The hospitalized patients are successfully treated and recovered at a rate γ_3. However, symptomatic and hospitalized individuals may have an associated disease-induced death rates δ_1 and δ_2. Natural death rate μ is associated to all the epidemiological compartments. Those in symptomatic infectious class have reduced infectiousness compared to asymptomatic infectious class at the rate η. The formulation of our model is guided by the flow-diagram in Fig. 1 and the following assumptions:

i. Individuals who received the first dose of the vaccine can revert back to the susceptible class as a result of the waning of the COVID-19 vaccine. This is supported by the report of WHO [7].
ii. Adhering to COVID-19 protocols on infection control and prevention can be enhanced via media campaign. This is in agreement with the reports in [47,48].
iii. There is permanent immunity after recovery. This is supported by the reports in [49].
iv. All infected classes are infectious but under ideal situations, both Quarantined and Hospitalized (Isolated) individuals have insignificant contact rate and hence assumed not to be part of the transmission dynamics. This is supported by the report of CDC [50].
v. The second dose of the vaccine further reduces the chances of infection. This is in line with the reports of [7,51].
vi. There is outbreak of infection among the first-dose vaccinated individuals. This is supported by the fact that first dose of COVID-19 vaccines only offers partial immunity [7,52].

The above description leads to the flow diagram in Fig. 1. Tables 1 and 2 show the values of the variables and parameters to be used in the model (1).

$$
\begin{aligned}
\frac{dS(t)}{dt} &= \Lambda + \omega V_1 - \tau_1\lambda S - (\rho_1+\mu)S,\\
\frac{dV_1(t)}{dt} &= \rho_1 S - \tau_2\lambda V_1 - (\omega+\rho_2+\mu)V_1,\\
\frac{dV_2(t)}{dt} &= \rho_2 V_1 - (\rho_3+\mu)V_2,\\
\frac{dL(t)}{dt} &= \lambda(\tau_1 S + \tau_2 V_1) - (\sigma+\theta+\gamma_1+\mu)L,\\
\frac{dQ(t)}{dt} &= \theta L - (\phi_1+\gamma_2+\mu)Q.\\
\frac{dI_a(t)}{dt} &= \sigma(1-\psi)L - (\phi_2+\xi+\mu)I_a,\\
\frac{dI_s(t)}{dt} &= \sigma\psi L + \xi I_a - (\phi_3+\delta_1+\mu)I_a,\\
\frac{dP(t)}{dt} &= \phi_1 Q + \phi_2 I_a + \phi_3 I_s - (\gamma_3+\delta_2+\mu)P,\\
\frac{dR(t)}{dt} &= \rho_3 V_2 + \gamma_1 L + \gamma_2 Q + \gamma_3 P - \mu R.
\end{aligned}
\tag{1}
$$

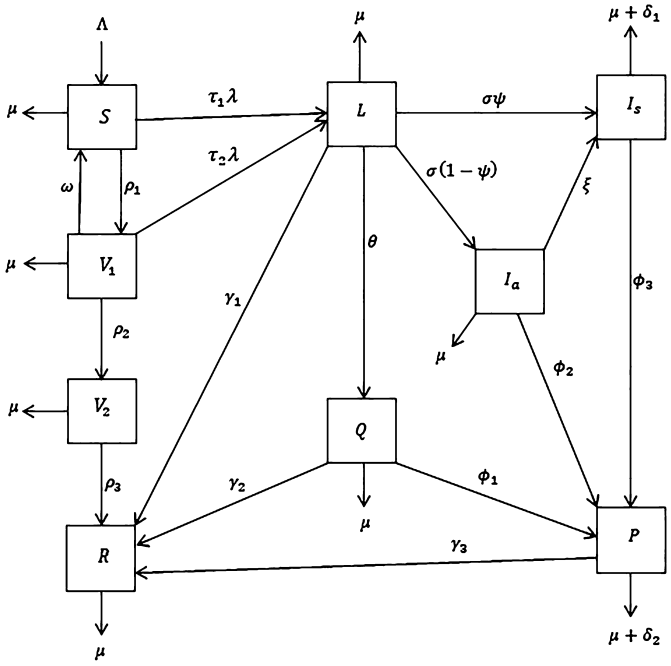

Fig. 1. Flow diagram of COVID-19 transmission dynamics with media campaign and double dose vaccination.

Table 1
Variables information.

Variable	Description	Value	Source
S	Susceptible individuals	176725630	estimated
V_1	First dose vaccinated individuals	17914944	[6]
V_2	Second dose vaccinated individuals	8197832	[6]
L	Latent individuals	4465192	estimated
Q	Quarantined individuals	4726096	Implied from NCDC [3]
I_a	Asymptomatic infectious individuals	4210002	estimated
I_s	Symptomatic infectious individuals	255190	Implied from NCDC [3]
P	Hospitalized (isolated) individuals	2572	Implied from NCDC [3]
R	Recovered individuals	249476	Implied from NCDC [3]
N	Total population	216746934	[53]

The model (1) satisfies the initial conditions: $S(0) = S_0, V_1(0) = V_{10}, V_2(0) = V_{20}, L(0) = L_0, Q(0) = Q_0, I_a(0) = I_{a0}, I_s(0) = I_{s0}, P(0) = P_0, P(0) = P_0$, and the force of infection λ, is given by

$$\lambda = \frac{c(1-\epsilon\varphi)(I_a + \eta I_s)}{N}, \tag{2}$$

where ϵ is the efficacy of media campaign and φ is the compliance of the campaign. c denotes the average number of contacts made and $N(t) = S(t) + V_1(t) + V_2(t) + L(t) + Q(t) + I_a(t) + I_s(t) + P(t) + R(t)$, is the total population size at time t.

Remark 1. The detail of the estimations of the initial values (in Table 1) and parameters (in Table 2) can be found in Appendix C.

3. Basic properties

Since the system (1) addresses human populations, it is assumed that the state variables and parameters are non-negative. It follows that the non-negative cone R^9_+, is invariant, as is the disease-free plane ($L = I_a = I_s = P = 0$). For convenience, we define $N^0 = \frac{\Lambda}{\mu}, S^0 = \frac{\Lambda(\omega+\rho_2+\mu)}{\mu(\omega+\rho_2+\mu)+\rho_1\rho_2}, V_1^0 = \frac{\Lambda\rho_1}{\mu(\omega+\rho_2+\mu)+\rho_1\rho_2}, V_2^0 = \frac{\Lambda\rho_1\rho_2}{(\rho_3+\mu)\left(\mu(\omega+\rho_2+\mu)+\rho_1\rho_2\right)}$ and $R^0 = \frac{\Lambda\rho_1\rho_2}{\mu(\rho_3+\mu)\left(\mu(\omega+\rho_2+\mu)+\rho_1\rho_2\right)}$. The rate of change of the total population, N is given by

$$\frac{dN}{dt} = \Lambda - \mu N - \delta_1 I_s - \delta_2 P. \tag{3}$$

Since the right hand side of the above equality is bounded by $\Lambda - \mu N$, a standard comparison theorem can be used to show that

$$N(t) \leq \frac{\Lambda}{\mu} + \left(N(0) - \frac{\Lambda}{\mu}\right)e^{-\mu t}.$$

It follows that

Table 2
Parameters information.

Parameter	Description	Value	Source
Λ	Recruitment rate	3901445	estimated
ρ_1	First dose vaccination rate	0.083	estimated
ρ_2	Second dose vaccination rate	0.038	estimated
ρ_3	Progression rate from V_2 to R	0.74	estimated
ω	Waning rate of first dose	0.67	estimated
μ	Natural death rate	0.0180	estimated
δ_1	The disease-induced death rate of I_a	0.0123	estimated
δ_2	The disease-induced death rate of P	0.002	estimated
(τ_1, τ_2)	COVID-19 transmission rates	(0.7, 0.33)	(estimated, [54])
c	Average contact rate	0.2	estimated
ϵ	Efficacy rate of media campaign	0.9	Assumed
φ	Rate of compliance to media campaign	0.5	Assumed
ϕ_1	Rate of hospitalization of Q	$5.4 \times 10^{-}4$	estimated
ϕ_2	Rate of hospitalization of I_a	$6.1 \times 10^{-}4$	estimated
ϕ_3	Rate of hospitalization of I_s	0.01	estimated
θ	Rate of quarantine of L to Q	0.022	estimated
η	Modification parameter	0.01	Assumed
σ	Disease progression rate	0.057	estimated
ψ	Proportion of L that goes to I_s	0.94	estimated
ξ	Progression rate from I_a to I_s	0.061	estimated
γ_1	Self-immune recovery rate of L individuals	0.903	estimated
γ_2	Self-immune recovery rate of Q individuals	0.95	estimated
γ_3	Recovery rate of P individuals due to treatment	0.98	estimated

$$0 < \limsup_{t \longmapsto \infty} N(t) \leq N^0,$$

with $\limsup_{t \longmapsto \infty} N(t) = N^0$ if and only if $\limsup_{t \longmapsto \infty} I_s(t) = \limsup_{t \longmapsto \infty} P(t) = 0$. From the first and second equations of model (1), we have that

$$0 < \limsup_{t \longmapsto \infty} S(t) \leq S^0, \tag{4}$$

and

$$0 < \limsup_{t \longmapsto \infty} V_1(t) \leq V_1^0. \tag{5}$$

Using equation (5) and the third equation of model (1), after little manipulation, we arrive at

$$0 < \limsup_{t \longmapsto \infty} V_2(t) \leq V_2^0, \tag{6}$$

and the last equation in (1) gives

$$0 < \limsup_{t \longmapsto \infty} R(t) \leq R^0. \tag{7}$$

It follows from equation (3) that if $N > N^0$, then $\frac{dN}{dt} < 0$. This proves the following lemma.

Lemma 3.1. *The closed set*

$$\Omega = \left\{ (S, V_1, V_2, L, Q, I_a, I_s, P, R) \in R_+^9 \,:\, N \leq N^0, V_1 \leq V_1^0, V_2 \leq V_2^0, R \leq R^0 \right\}$$

is a positively invariant and attracting region of system (1) with initial conditions in R_+^9.

Thus, in the absence of COVID-19 ($L = I_a = I_s = P = 0$), the total population, N, approaches the carrying capacity, N^0, asymptotically; and in the presence of the pandemic, the total population is less than or equal to N^0. That means, any phase trajectory initiated anywhere in the non-negative region $R_+^9 \geq 0$ of the phase space eventually enters the domain Ω and remains in it. If $N(0) \leq \frac{\Lambda}{\mu}$, then $N(t) \leq \frac{\Lambda}{\mu}$. Therefore, Ω is a positively invariant set under the flow described in model (1). Hence, no solution path leaves through any boundary of Ω. The right hand side of model (1) is smooth, hence the initial value problem has a unique solution that exists on maximal intervals [55]. Since paths cannot leave the set Ω, solutions remain non-negative for non-negative initial conditions, the solutions exist at all positive time. Thus, the system (1) is mathematically and epidemiologically well posed [55].

4. The disease-free equilibrium

4.1. Existence and local stability of disease-free equilibrium (DFE)

The model (1) has a DFE, obtained by setting the right hand side of the equations to zero, given by

$$E_0 = (S^0, V_1^0, V_2^0, L^0, Q^0, I_a^0, I_s^0, P^0, R^0)$$
$$= \Big(\frac{\Lambda(\omega+\rho_2+\mu)}{\mu(\omega+\rho_2+\mu)+\rho_1\rho_2}, \frac{\Lambda\rho_1}{\mu(\omega+\rho_2+\mu)+\rho_1\rho_2}, \frac{\Lambda\rho_1\rho_2}{(\rho_3+\mu)\Big(\mu(\omega+\rho_2+\mu)+\rho_1\rho_2\Big)}, 0, 0, 0, 0, 0, \frac{\Lambda\rho_1\rho_2}{\mu(\rho_3+\mu)\Big(\mu(\omega+\rho_2+\mu)+\rho_1\rho_2\Big)}\Big).$$

The stability of E_0 can be established using the next generation matrix on the system (1). Using the symbols in van den Dressiche and Watmough [56], the matrices F and V, for the new infections and the remaining transfer terms respectively, are given by

$$F = \begin{pmatrix} 0 & 0 & \frac{c(1-\epsilon\varphi)(\tau_1 S^0+\tau_2 V_1^0)}{N^0} & \frac{c(1-\epsilon\varphi)\eta(\tau_1 S^0+\tau_2 V_1^0)}{N^0} & 0 \\ 0 & 0 & 0 & 0 & 0 \\ 0 & 0 & 0 & 0 & 0 \\ 0 & 0 & 0 & 0 & 0 \\ 0 & 0 & 0 & 0 & 0 \end{pmatrix}$$

and

$$V = \begin{pmatrix} \sigma+\theta+\gamma_1+\mu & 0 & 0 & 0 & 0 \\ -\theta & \phi_1+\gamma_2+\mu & 0 & 0 & 0 \\ -\sigma(1-\psi) & 0 & \phi_2+\xi+\mu & 0 & 0 \\ -\sigma\psi & 0 & -\xi & \phi_3+\delta_1+\mu & 0 \\ 0 & -\phi_1 & -\phi_2 & -\phi_3 & \gamma_3+\delta_2+\mu \end{pmatrix}.$$

Thus,

$$R_{mv} = (1-\epsilon\varphi)R_v, \tag{8}$$

where

$$R_v = \frac{c\sigma\mu\Big((\phi_3+\delta_1+\mu)(1-\psi)+\eta(\xi(1-\psi)+(\phi_2+\xi+\mu)\psi)\Big)(\tau_1(\omega+\rho_2+\mu)+\tau_2\rho_1)}{(\sigma+\theta+\gamma_1+\mu)(\phi_2+\xi+\mu)(\phi_3+\delta_1+\mu)(\mu(\omega+\rho_2+\rho_1+\mu)+\rho_1\rho_2)}, \tag{9}$$

is the vaccination-induced reproduction number, determined by setting $(\epsilon,\varphi)=0$ and media-induced reproduction number, R_m, can be obtained by setting vaccination related parameters to zero as given (11)

$$R_m = (1-\epsilon\varphi)R_0, \tag{10}$$

with

$$R_0 = \frac{c\sigma\tau_1\Big[(\delta_1+\mu)(1-\psi)+\eta\Big(\xi(1-\psi)+(\xi+\mu)\psi\Big)\Big]}{(\sigma+\gamma_1+\mu)(\xi+\mu)(\delta_1+\mu)}, \tag{11}$$

as the basic reproduction number considered when there are no controls. The basic reproduction number, traditionally denoted by R_0, is the average number of secondary infections produced by a single infected individual during its entire infectious period when introduced in a population where everyone is susceptible [57,58]. Note that R_{mv} is obtained from $\rho\Big(FV^{-1}\Big)$ with ρ being the spectral radius of the next generation matrix FV^{-1} [56]. In order to determine the dynamics of COVID-19 over time, there is need to compute R_{mv}. The value of the threshold quantity R_{mv} shows the risk in transmission of the disease in the midst of media campaigns and double-dose vaccination strategies. By the definitions and the expressions above, it is obvious that $R_{mv} < R_o$ always hold. That means, maintaining R_{mv} always below R_0 will bring COVID-19 cases under control and subsequently stop possible spread. The following result follows from Theorem 2 of van den Dressiche and Watmough [56].

Lemma 4.1. *The DFE of the model (1), E_0, is locally asymptotically stable if $R_{mv} < 1$ and unstable if $R_{mv} > 1$.*

The threshold quantity R_{mv} is the control reproduction number for the COVID-19 transmission dynamics. In biological sense, Lemma 4.1 implies that COVID-19 can be eliminated from the population (when $R_{mv} < 1$) if the initial sizes of the populations of the model are in the basin of attraction of E_0.

The parameter $f_e = \epsilon\varphi$, where ϵ and φ denote the media campaign efficacy and compliance, respectively. Let $f_e = \epsilon\varphi$ be the media-induced preventability of COVID-19 transmission. Thus, the reproduction number of the model with media only as control measure can be expressed as in equation (10). It explains the impact of media campaign in preventing COVID-19 transmission. We noticed that $R_m(0,\varphi) = R_m(\epsilon,0) = R_m(0,0) = R_0$ and that $R_m(\epsilon,\varphi) \le R_0 \quad \forall \epsilon,\varphi \ge 0$. Therefore, the basic reproduction number (in the absence of media campaign and vaccination) R_0 is greater than the media-induced reproduction number ($R_0 > R_m$). Thus, the use of media campaign as a preventive measure can limit the spread of COVID-19 in a population. As in Malunguza et al. [59] the proof of Lemma 4.2 follows.

Lemma 4.2. *COVID-19 can be eliminated from the population if the preventability $f_e = \epsilon\varphi$ exceeds the threshold value f_e^*.*

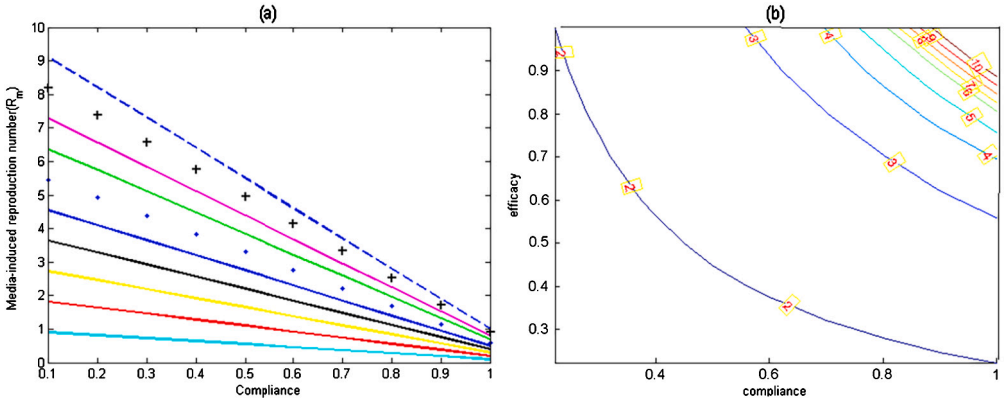

Fig. 2. Simulation results showing patterns of R_m against compliance, φ on the left and on the right, the contours of $R_m = (1-\epsilon\varphi)R_0 = 1$ with respect to efficacy, ϵ and compliance. The corresponding values of R_m are obtained by varying values of R_0 from 1 to 10 in step 1 and ϵ, φ from 0.1 to 1 in the step of 0.1 using parameter values in Table 1 and $c = 2$.

Proof. It follows from equation (10) that

$$R_m = (1-\epsilon\varphi)R_0 \le 1, \epsilon \ge \frac{1}{\varphi}\left(1-\frac{1}{R_0}\right) = \epsilon^*, \tag{12}$$

then $R_m(\epsilon^*) = 1$ assuming $\varphi > 0$. If

$$\varphi^* = \frac{1}{\epsilon}\left(1-\frac{1}{R_0}\right), \tag{13}$$

then $R_m(\varphi^*) = 1$ assuming $\epsilon > 0$. Note that $\epsilon^*(\varphi^*)$ is critical value that shows the minimum rate of media coverage (compliance) in a community where COVID-19 vaccines and other interventions are not available. Since R_m is a decreasing function of both ϵ and φ, it follows that $R_m < 1$ whenever $\epsilon > \epsilon^*$ or $\varphi > \varphi^*$. It is also important to note that R_m is as well a decreasing function of f_e. This means that COVID-19 pandemic can be eliminated in the population if $f_e > f_e^* = \epsilon^*\varphi^*$. □

4.2. Impact of media campaign on R_0

The media-induced reproduction number R_m is given in terms of R_0 as in equation (10). Therefore, we write $R_m = R_m(R_0)$ to show the dependence of R_m on R_0. The obtained results in Fig. 2 show that there are certain values of R_0 for which the presence of media campaign may not necessarily reduce R_m to values less than unity, even if 100% compliance to public health policies is achieved. Furthermore, we noticed that when $R_0 = 7$, we have $R_m = 1.015$ at $\varphi = 0.95$. This implies that with high compliance value ($\varphi > 0.9$) in a community, the control of COVID-19 may not be possible with the use of media campaign alone as a preventive strategy.

Since $R_{mv} \le 1$ is a necessary and sufficient condition for the disease elimination (Lemma 4.1 and Theorem 4.4), it follows that the above conditions on ϵ (in equation (12) is also necessary and sufficient condition for control. Therefore, the inequality (8) can be rewritten as

$$\epsilon\varphi \ge 1 - \frac{1}{R_0}.$$

It follows that with $R_0 = 4$, the pandemic control requires the product of $\epsilon\varphi$ greater than $\frac{3}{4}$ as shown in the upper region of the right plot of Fig. 2. In order to exceed this target, both ϵ and φ must be greater than $\frac{3}{4}$. In summary, this study reveals that if $R_0 = 4$, at least 75% media coverage and compliance on COVID-19 control and prevention guidelines is needed in the community to attain herd immunity. This is contrary to the report by Ram and Schaposnik [60] that says COVID-19 herd immunity can be attained at 82% for $R_0 = 5.7$.

4.3. Impact of media campaign and double dose vaccination on R_{mv}

In analogous fashion to Lemma 4.2, we state and prove the following result.

Lemma 4.3. *COVID-19 can be eliminated from the community if the preventability $f_\alpha = \epsilon_\alpha\varphi_\alpha$, where $\epsilon = \epsilon_\alpha$ and $\varphi = \varphi_\alpha$ in (8) is greater than the threshold value $f_\alpha^* = \epsilon_\alpha^*\varphi_\alpha^*$.*

Proof. As in Lemma 4.2, if

$$R_{mv} = (1-\epsilon_\alpha\varphi_\alpha)R_v \le 1, \epsilon_\alpha \ge \frac{1}{\varphi_\alpha}\left(1-\frac{1}{R_v}\right) = \epsilon_\alpha^*, \tag{14}$$

then $R_{mv}(\epsilon_\alpha^*) = 1$ supposing that $\varphi_\alpha > 0$. Again, if

$$\varphi_\alpha^* = \frac{1}{\epsilon_\alpha}\left(1-\frac{1}{R_v}\right), \tag{15}$$

then $R_{mv}(\varphi_\alpha^*) = 1$ supposing that $\epsilon_\alpha > 0$. Hence, the conclusion of the result follows from Lemma 4.2. □

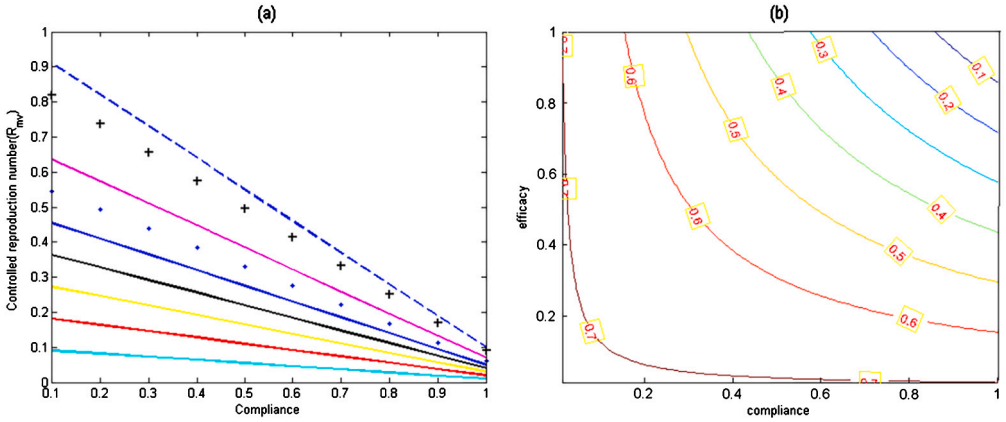

Fig. 3. Simulation results showing (a) patterns of R_{mv} against compliance, φ and (b) the contours of R_{mv} in (8) with respect to media efficacy, ϵ and compliance. The corresponding values of R_{mv} are obtained by varying values of R_m and (ϵ, φ) from 0.1 to 1 in the step 0.1 using parameter values in Table 2 and $c = 2$.

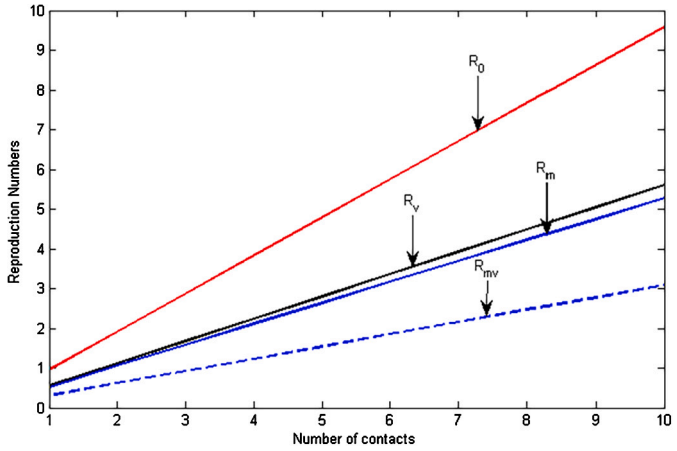

Fig. 4. Simulation results showing the patterns of the reproduction numbers R_{mv}, R_m, R_v, R_0 for varying number of contacts from 1 to 10. Parameters used are $\eta = 0.3, \psi = 0.094$ and others are as in Table 2.

As in subsection 4.3, we write $R_{mv} = R_{mv}\left[(1-\epsilon\varphi)R_v\right]$ as a function that illustrates the dependence of R_{mv} on $(1-\epsilon\varphi)R_v$. The simulated results are depicted in Fig. 3. It is observed in Fig. 3(a) that the controlled reproduction number, R_{mv}, does not increase above unity in the presence of varying compliance and vaccination-induced reproduction number, R_v within 0 to 1. This means that the combination of media compliance with vaccination has a greater potential of eradicating COVID-19 from the community faster than implementing either media campaign or double dose vaccination alone as a control measure. The contours of R_{mv} with respect to media efficacy and compliance as R_v varies, clearly shows that $R_{mv} < 1$ when media campaign and its compliance are intensified in the community. Therefore, to achieve COVID-19-free society, compliance with public health policies such as wearing of face masks, maintaining social distancing, regular washing of hands and receiving of first and second doses of COVID-19 vaccine should be encouraged among the populace. Note also from Fig. 3b that, a corresponding increase in efficacy and compliance to media campaign reduces R_{mv} to a value below unity. However, a high efficacy with low compliance and vice-versa may not eliminate COVID-19 in the community sufficiently.

For clarity of doubt, we illustrate the relationship and behaviour among the reproduction numbers R_{mv}, R_m, R_v and R_0 with respect to increasing the number of contacts (c). We observed in Fig. 4 that the four reproduction numbers satisfy the inequality $R_{mv} < R_m < R_v < R_0$. The results further affirm that the use of media campaign and vaccination is far better than implementing single controls (R_m, R_v). However, for single controls, $R_m < R_v$ implies that media is more beneficial in controlling the spread of COVID-19 than vaccination. Of course, the inequality shows a worse scenario in the outbreak of the pandemic where none of the controls are applied.

4.4. Global stability of DFE

Theorem 4.4. *The DFE of the model (1), E_0, is globally asymptotically stable if $R_{mv} \leq 1$.*

Proof. Using the method of Hntsa and Kahsay [61], consider a Lyapunov function $\Theta_f = L$. From the equations in model (1), setting $\frac{dQ}{dt} = \frac{dL_a}{dt} = \frac{dI_s}{dt} = \frac{P}{dt} = 0$, we have the following:

$$Q = \frac{\theta L}{k_5},$$

$$I_a = \frac{\sigma(1-\psi)L}{k_6},$$

$$I_s = \frac{\sigma(\psi k_6 + \xi(1-\psi))L}{k_6 k_7}, \tag{16}$$
$$P = \frac{\left[\phi_1 \theta k_6 k_7 + \phi_2 k_5 \sigma(1-\psi)k_7 + \phi_3 k_5 \sigma(\psi k_6 + \xi(1-\psi))\right]L}{k_5 k_6 k_7 k_8}.$$

Taking the derivative of Θ_f gives

$$\begin{aligned} \frac{d\Theta_f}{dt} &= \frac{dL}{dt} = \lambda(\tau_1 S + \tau_2 V_1) - k_4 L, \\ &= (B_1 I_a + B_2 I_s)\frac{S}{N} + (B_3 I_a + B_4 I_s)\frac{V_1}{N} - k_4 L, \end{aligned} \tag{17}$$

where $B_1 = \tau_1 c(1-\epsilon\varphi)$, $B_2 = \tau_1 c\eta(1-\epsilon\varphi)$, $B_3 = \tau_2 c(1-\epsilon\varphi)$ and $B_4 = \tau_2 c\eta(1-\epsilon\varphi)$. Substituting (16) into (17) gives

$$\frac{d\Theta_f}{dt} = \left[\left(\frac{B_1\sigma(1-\psi)}{k_6} + \frac{B_2\sigma(\psi k_6 + \xi(1-\psi))L}{k_6 k_7}\right)\frac{S}{N} + \left(\frac{B_3\sigma(1-\psi)}{k_6} + \frac{B_4\sigma(\psi k_6 + \xi(1-\psi))}{k_6 k_7}\right)\frac{V_1}{N} - k_4\right]L. \tag{18}$$

Recall that at DFE,

$$\frac{S}{N} \le \frac{S_0}{N^0} = \frac{\mu k_2}{\mu(\omega + \rho_1 + \mu) + \rho_2 k_1} = B_5 \quad \text{and} \quad \frac{V_1}{N} \le \frac{V_1^0}{N^0} = \frac{\mu\rho_1}{\mu(\omega + \rho_1 + \mu) + \rho_2 k_1} = B_6.$$

Thus, letting $B_7 = B_1 B_5 + B_3 B_6$ and $B_8 = B_2 B_5 + B_4 B_6$, we have

$$\begin{aligned} \frac{d\Theta_f}{dt} &\le \left[\frac{\sigma(1-\psi)}{k_6}(B_1 B_5 + B_3 B_6) + \frac{\sigma(\psi k_6 + \xi(1-\psi))}{k_6 k_7}(B_2 B_5 + B_4 B_6) - k_4\right]L \\ &\le \left[\left(\frac{\sigma(1-\psi)k_7 B_7 + B_8\sigma(\psi k_6 + \xi(1-\psi))L}{k_6 k_7}\right) - k_4\right]L \\ &\le k_4\left(\frac{\sigma(1-\psi)k_7 B_7 + B_8\sigma(\psi k_6 + \xi(1-\psi))L}{k_4 k_6 k_7} - 1\right)L \\ &\le k_4\left(R_{mv} - 1\right)L. \end{aligned} \tag{19}$$

The values of $k_i, i = 1, 2, ..., 8$ are given by equation (20)

$$\begin{aligned} &k_1 = (\rho_1 + \mu), k_2 = (\omega + \rho_2 + \mu), k_3 = (\rho_3 + \mu), \\ &k_4 = (\sigma + \theta + \gamma_1 + \mu), k_5 = (\phi_1 + \gamma_2 + \mu), k_6 = (\phi_2 + \xi + \mu), \\ &k_7 = (\phi_3 + \delta_1 + \mu), k_8 = (\gamma_3 + \delta_2 + \mu). \end{aligned} \tag{20}$$

It is clear from (19) that $\frac{d\Theta_f}{dt} \le 0$ (negative semi-definite) when $R_{mv} \le 1$ and equality holding when $R_{mv} = 1$. Therefore, the largest compact set Ω such that $\frac{d\Theta_f}{dt} = 0$ when $R_{mv} \le 1$ is the singleton E_0. Hence, by La Salle invariance principle [62], the DFE is globally asymptotically stable in Ω. □

5. Uniform persistence and existence of endemic equilibrium

5.1. Uniform persistence

The uniform persistence of the disease will now be established in the context of the model (1). That is, the objective is to determine whether or not the number of infectious cases in the population will persist above a certain positive number for a long time period considering the case when $R_{mv} > 1$.

Definition 5.1. Model (1) is said to be uniformly persistent [57,63] if there exists a constant $0 < \varpi < 1$, independent of the initial data in $\bar{\Omega}$, such that, any solution $x(t) = \left(S(t), V_1(t), V_2(t), L(t), Q(t), I_a(t), I_s(t), P(t), R(t)\right)$ of model (1) satisfies

$$\begin{aligned} &lim_{t\mapsto\infty} inf\, S(t) \ge \varpi, lim_{t\mapsto\infty} inf\, V_1(t) \ge \varpi, lim_{t\mapsto\infty} inf\, V_2(t) \ge \varpi, \\ &lim_{t\mapsto\infty} inf\, L(t) \ge \varpi, lim_{t\mapsto\infty} inf\, Q(t) \ge \varpi, lim_{t\mapsto\infty} inf\, I_a(t) \ge \varpi, \\ &lim_{t\mapsto\infty} inf\, I_s(t) \ge \varpi, lim_{t\mapsto\infty} inf\, P(t) \ge \varpi, lim_{t\mapsto\infty} inf\, R(t) \ge \varpi, \end{aligned}$$

provided $x(0) \in \bar{\Omega}$.

To study the uniform persistence of our model, we need the following result:

Lemma 5.2. *If $R_{mv} > 1$, then the model system (1) is uniformly persistent and there exists atb least one endemic equilibrium in $\bar{\Omega}$.*

Proof. When $R_{mv} > 1$, then by utilizing the Lyapunov function in Theorem 4.4 one can easily see that E_0 is unstable. Actually, if $R_{mv} > 1$, then the derivative of the Lyapunov function $\frac{d\Theta_f}{dt} > 0$ for S, V_1, V_2 and R sufficiently close to S^0, V_1^0, V_2^0 and R^0, respectively, except when $L = 0$. Therefore, $R_{mv} > 1$ all the solution trajectories beginning from E_0 must leave the neighbourhood of E_0, except those on the positively invariant $\Omega-$ axis. Thus, E_0 have no $\omega-$ limit point of any orbit beginning in the boundary of Ω. By using Theorem 4.3 in [64], and similar arguments in (Lemma 1 [57], Theorem 3.5 [65], Theorem 5.2 [63]), we can assert that, when $R_{mv} > 1$, the instability of E_0 implies the uniform persistence of model (1). The

uniform persistence and the positive invariance of the compact set Ω imply the existence of an endemic equilibrium in $\bar{\Omega}$ (see Theorem 2.2 in [66]). □

5.2. Existence of endemic equilibrium, E^*

Let $E^* = (S^*, V_1^*, V_2^*, L^*, Q^*, I_a^*, I_s^*, P^*, R^*)$ be the endemic equilibrium of the model (1). Then after setting the system to zero and evaluating in terms of force of infection λ, we have

$$\begin{aligned}
&S^* = \frac{\Lambda(k_2+\tau_2\lambda)}{\upsilon_1+\upsilon_2\lambda+\tau_1\tau_2\lambda^2}, V_1^* = \frac{\Lambda\rho_1}{\upsilon_1+\upsilon_2\lambda+\tau_1\tau_2\lambda^2}, V_2^* = \frac{\Lambda\rho_1\rho_2}{\upsilon_1+\upsilon_2\lambda+\tau_1\tau_2\lambda^2},\\
&L^* = \frac{\lambda(m_0+\tau_1\tau_2\lambda)\Lambda}{k_4(\upsilon_1+\upsilon_2\lambda+\tau_1\tau_2\lambda^2)}, Q^* = \frac{\lambda(m_0+\tau_1\tau_2\lambda)\Lambda\theta}{k_4k_5(\upsilon_1+\upsilon_2\lambda+\tau_1\tau_2\lambda^2)}, I_a^* = \frac{\lambda(m_0+\tau_1\tau_2\lambda)\Lambda\sigma_m}{k_4k_6(\upsilon_1+\upsilon_2\lambda+\tau_1\tau_2\lambda^2)},\\
&I_s^* = \frac{\lambda(m_0+\tau_1\tau_2\lambda)\Lambda\phi_\sigma}{k_4k_6k_7(\upsilon_1+\upsilon_2\lambda+\tau_1\tau_2\lambda^2)}, P^* = \frac{\lambda(m_0+\tau_1\tau_2\lambda)\Lambda F_\theta}{k_4k_5k_6k_7k_8(\upsilon_1+\upsilon_2\lambda+\tau_1\tau_2\lambda^2)},\\
&R^* = \frac{(a_1+b_1\lambda+c_1\lambda^2)\Lambda}{\mu k_3k_4k_5k_6k_7k_8(\upsilon_1+\upsilon_2\lambda+\tau_1\tau_2\lambda^2)},
\end{aligned} \tag{21}$$

and the total population at endemic gives

$$N^* = \frac{(f_0+f_1\lambda+f_2\lambda^2)\Lambda}{\mu\prod_{i=3}^{8}k_i(\upsilon_1+\upsilon_2\lambda+\tau_1\tau_2\lambda^2)}, \tag{22}$$

where the k_i parameters are as defined by equation (20), and others as in (23)

$$\begin{aligned}
&\upsilon_1 = \mu(k_2+\rho_1)+\rho_1\rho_2, \upsilon_2 = k_1\tau_2+k_2\tau_1, m_0 = k_2\tau_1+\rho_1\tau_2, \sigma_m = \sigma(1-\psi),\\
&\sigma_n = \sigma\psi, \phi_\sigma = \xi\sigma_m+k_6\sigma_n, F_\theta = \theta k_6k_7\phi_1+k_5k_7\phi_2\sigma_m+k_5\phi_3\phi_\sigma, a_1 = \rho_1\rho_2\rho_3\prod_{i=4}^{8}k_i,\\
&b_1 = k_3k_6k_7k_8(\gamma_1k_5+\theta\gamma_2)m_0+\gamma_3k_3k_5\phi_3m_0\phi_\sigma+\gamma_3k_3k_7(\theta k_6\phi_1+k_5\phi_2\sigma_m)m_0,\\
&c_1 = \tau_1\tau_2\gamma_3k_3k_5\phi_3\phi_\sigma+\tau_1\tau_2k_3k_6k_7k_8(\theta\gamma_2+\gamma_1k_3)+\tau_1\tau_2\gamma_3k_3k_7(k_5\phi_2\sigma_m+\theta k_6\phi_1),\\
&f_2 = \mu\tau_1\tau_2k_3k_6k_7k_8(\theta+k_5)+\mu\tau_1\tau_2k_3k_5k_8(k_7\sigma_m+\phi_\sigma)+\mu\tau_1\tau_2k_3F_\theta+c_1,\\
&f_1 = \mu\tau_2\prod_{i=3}^{8}k_i+\mu k_3k_6k_7k_8m_0(\theta+k_5)+\mu k_3k_5k_8m_0(k_7\sigma_m+\phi_\sigma)+\mu k_3m_0F_\theta+b_1,\\
&f_0 = \upsilon_1\prod_{i=3}^{8}k_i.
\end{aligned} \tag{23}$$

Substituting the expressions in equations (21) and (22) into (2), and simplifying yields the following quadratic in terms of λ:

$$G(\lambda) = G_2\lambda^2+G_1\lambda+G_0, \tag{24}$$

where

$$\begin{aligned}
&G_2 = f_2k_4k_6k_7,\\
&G_1 = f_1k_4k_6k_7\Big[1-g(\tau)R_{mv}\Big], g(\tau) = (\frac{\upsilon_1}{m_0})(\frac{\tau_1\tau_2}{f_1}),\\
&G_0 = f_0k_4k_6k_7\Big[1-R_{mv}\Big].
\end{aligned} \tag{25}$$

The endemic equilibria of the model are given by equation (21) with λ^* a positive root of equation (24). Noting that negative endemic equilibria are biologically meaningless, the conditions for $G(\lambda)$ to have positive real roots are determined below.

It is clear that $G_2 > 0$ and so the quadratic $G(\lambda)$ is concave up. We now carry out case analysis to determine the number of positive real zeros of $G(\lambda)$.

Case a. Assume that $R_{mv} > 1$. Then $G_0 < 0$ and hence the vertical intercept of $G(\lambda)$ is negative. In addition to the fact that $G(\lambda)$ is a quadratic which concave upwards, it follows that $G(\lambda)$ has two real roots with opposite signs. Therefore, a unique positive equilibrium of the model exists whenever $R_{mv} > 1$.

Case b. Assume that $R_{mv} = 1$. Then $G_0 = 0$ and so the quadratic $G(\lambda)$ reduces to $G(\lambda) = \lambda(G_2\lambda+G_1)$, with roots $\lambda^* = 0$ (for the situation arising at DFE) and $\lambda^* = -\frac{G_1}{G_2}$. However, it is obvious from equation (25), that supposing $g(\tau) < 1$, then $G_1 \geq 0$ for $R_{mv} = 1$. Hence, no positive endemic equilibrium occurs for $R_{mv} = 1$.

Case c. Assume that $R_{mv} < 1$. Then $G_2, G_1, G_0 > 0$ when the effect of vaccination and outbreak of infection among individuals in class V_1 is ignored. Therefore, it is obvious that no positive real root occurs for $R_{mv} < 1$. This has ruled out the possibility of backward bifurcation.

Note case c also follows from Theorem 4.4, since global stability of DFE implies that there are no other equilibria. Hence, we have the following result.

Proposition 5.3. *For the case where vaccination impacts are ignored, then model (1) has a unique endemic equilibrium whenever $R_{mv} > 1$ and no positive endemic equilibrium when $R_{mv} \leq 1$.*

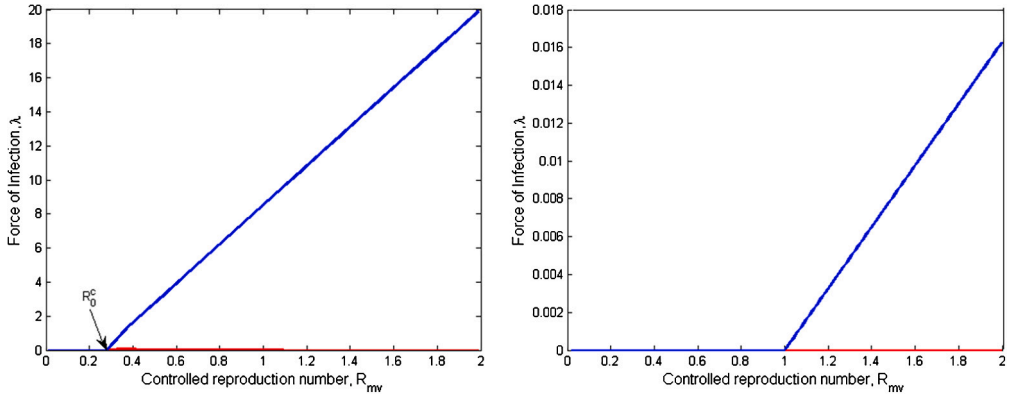

Fig. 5. The figure depicts the bifurcation diagram showing on the right the case of impact of vaccination and break-through of infection ($\tau_2 = 0.3, \rho_1 = \rho_2 = \rho_3 \neq 0.00$); and without impact of vaccination and breakthrough of infection ($\rho_1 = \rho_2 = \rho_3 = \tau_2 = 0.00$) on the left.

5.3. Bifurcation analysis

As in [67], we will use the centre manifold theory to determine the direction of bifurcation for the COVID-19 model (1) in Theorem 5.4.

Theorem 5.4. *If* $w_i < \frac{x_i^* B^*}{2N^*}$, *for* $i = 1, 2$, *then* $a < 0$ *and the model system (1) will undergo a forward bifurcation in the absence of vaccination effects* ($\rho_1 = \rho_2 = \rho_3 = \tau_2 = 0$). *Otherwise a backward bifurcation may occur.*

Proof. The proof of Theorem 5.4 follows from centre manifold theory as proved in Appendix A. □

Since $a < 0$ (from Theorem 5.4) and $b > 0$, the COVID-19 model (1) does not undergo backward bifurcation at $R_{mv} = 1$. That is, the DFE does not co-exist with stable endemic equilibrium. Hence, following similar conclusion of Goudiby et al. [68], we obtain the following result.

Theorem 5.5. *In the absence of vaccination, the unique endemic equilibrium of model (1) for model (1) is globally asymptotically stable if* $R_{mv} > 1$.

The above result when $R_{mv} > 1$ is shown graphically in Fig. 5. The red line in Fig. 5 represents the instability area of the disease-free equilibrium, E_0, and the blue line is the stability area of DFE and the endemic before and after the threshold stability switch line and $R_{mv} = R_0^c < 1$ and $R_{mv} = 1$ respectively. When $R_{mv} > 1$, the blue line moves upwards, hence, the endemic equilibrium E^* is globally asymptotically stable.

6. Optimal control system

An optimal control is a branch of mathematics that comes into play seeking for optimal ways of controlling infectious diseases in the midst of limited resources. In this section, an analysis to determine an optimal control strategy depends on three controls, compliance to media campaign, first dose vaccination and second-dose vaccination will be carried out. It is assumed that the media compliance rate φ, first-dose vaccination rate ρ_1 and second-dose vaccination rate ρ_2 are now time dependent, and will therefore act as control variables. Using these controls, the model in (1) becomes

$$\begin{aligned}
\frac{dS(t)}{dt} &= \Lambda + \omega V_1 - \frac{\tau_1 c(1-\epsilon\varphi(t))(I_a+\eta I_s)}{N} S - (\rho_1(t)+\mu)S,\\
\frac{dV_1(t)}{dt} &= \rho_1(t)S - \frac{\tau_2 c(1-\epsilon\varphi(t))(I_a+\eta I_s)}{N} V_1 - (\omega+\rho_2(t)+\mu)V_1,\\
\frac{dV_2(t)}{dt} &= \rho_2(t)V_1 - (\rho_3+\mu)V_2,\\
\frac{dL(t)}{dt} &= \frac{\tau_1 c(1-\epsilon\varphi(t))(I_a+\eta I_s)}{N} S + \frac{\tau_2 c(1-\epsilon\varphi(t))(I_a+\eta I_s)}{N} V_1 - (\sigma+\theta+\gamma_1+\mu)L,\\
\frac{dQ(t)}{dt} &= \theta L - (\phi_1+\gamma_2+\mu)Q.\\
\frac{dI_a(t)}{dt} &= \sigma(1-\psi)L - (\phi_2+\xi+\mu)I_a,\\
\frac{dI_s(t)}{dt} &= \sigma\psi L + \xi I_a - (\phi_3+\delta_1+\mu)I_a,\\
\frac{dP(t)}{dt} &= \phi_1 Q + \phi_2 I_a + \phi_3 I_s - (\gamma_3+\delta_2+\mu)P,\\
\frac{dR(t)}{dt} &= \rho_3 V_2 + \gamma_1 L + \gamma_2 Q + \gamma_3 P - \mu R.
\end{aligned} \tag{26}$$

For this, we consider the objective functional

$$J\left[\varphi, \rho_1, \rho_2\right] = \int_0^{t_f} \left[m_1 I_a + m_2 I_s + \frac{1}{2}\left(m_3\varphi^2(t) + m_4\rho_1^2(t) + m_5\rho_2^2(t)\right)\right] dt, \tag{27}$$

where the parameters m_1, m_2, m_3, m_4 and m_5 are the weight factors to help balance each term in the integrand in (27), so that none of the terms dominates. The terms in the integrand in (27) are explained as follows:

i. The term $m_1 I_a + m_2 I_s$ represents the cost associated with monitoring infected individuals in all stages (asymptomatic and symptomatic).
ii. The term $m_3\varphi^2(t)$ represents the cost associated with media campaign to educate the public on COVID-19 safety protocols.
iii. The terms $m_4\rho_1^2(t)$ and $m_5\rho_2^2(t)$ represents the cost associated with the first and second doses of vaccination, respectively.

Our aim is to minimize the total number of infected individuals while ensuring that the cost associated with the controls is minimized. The goal is to find an optimal control triplet $(\varphi^*(t), \rho_1^*(t), \rho_2^*(t))$, such that;

$$J\left[\varphi^*, \rho_1^*, \rho_2^*\right] = \underbrace{min}_{(\varphi,\rho_1,\rho_2)\in\Omega_p^0} J\left[\varphi, \rho_1, \rho_2\right], \tag{28}$$

where

$$\Omega_p^0 = \left\{ (\varphi(t), \rho_1(t), \rho_2(t)) \in L^1(0, t_f) \mid a_1 \le \varphi(t) \le b_1, a_2 \le \rho_1(t) \le b_2, a_3 \le \rho_2(t) \le b_3 \right\}$$

6.1. Analysis of the optimal control system

6.1.1. Existence of optimal control

In this subsection, we verify the existence of the optimal solution of the optimal solution of the model (26) with respect to the objective functional (27). The existence of the control triplet $(\varphi^*(t) = u_1^*, \rho_1^*(t) = u_2^*, \rho_2^*(t) = u_3^*)$ is guaranteed in the set

$$\Gamma = \left\{ u_i \quad \text{is measurable}, \quad 0 \le u_i \le 1 \quad \text{for} \quad t \in [0, t_f], i = 1, 2, 3 \right\},$$

which minimizes the cost functional J.

Theorem 6.1. *There exist optimal controls u_1^*, u_2^* and u_3^* in Γ associated with the optimal control problem (26) and (27) within the fixed interval $\left[0, t_f\right]$.*

Proof. We follow the procedure and utilize the results in the works of [5,69] to prove the theorem. To ascertain the existence of optimal controls, the under listed conditions must be satisfied:

(a) the boundedness of the solution of the optimal control (26) confirms the existence of the solution of system (26);
(b) the optimal control set and the associated state variables are non-empty;
(c) the solution of the system (26) is bounded above by a linear function in the control as well as state variables;
(d) the integrand in the cost functional J, $L(I_a, I_s, u_i) = m_1 I_a + m_2 I_s + \frac{m_3}{2}u_1^2(t) + \frac{m_4}{2}u_2^2 + \frac{m_5}{2}u_3^2$ is convex on the control set Γ;
(e) there exist constants b_1, b_2 and $q > 0$ such that

$$m_1 I_a + m_2 I_s + \frac{m_3}{2}u_1^2(t) + \frac{m_4}{2}u_2^2 + \frac{m_5}{2}u_3^2 \le b_1 + b_2\Big(\sum_{i=1}^{3}|u_i|^2\Big)^{\frac{q^*}{2}},$$

where b_1 depends upon upper bounds of I_a and I_s, and $b_2 = \frac{max}{2}\{m_3, m_4, m_5\}$ and $q^* = 2$. □

6.1.2. Characterization of optimal control

We apply the Pontryagin's Maximum Principle as in Gweryina et al. [35] to find the necessary conditions for the optimal controls. This Principle converts equations (26) and (27) into a problem of minimizing point-wise Hamiltonian, with respect to the controls $\varphi(t), \rho_1(t)$ and $\rho_2(t)$. The Hamiltonian is given by;

$$\begin{aligned}
H = {} & m_1 I_a + m_2 I_s + \frac{1}{2}\Big(m_3\varphi^2(t) + m_4\rho_1^2(t) + m_5\rho_2^2(t) + \lambda_!^*\Big[\Lambda + \omega V_1 - \frac{\tau_1 c(1-\epsilon\varphi(t))(I_a+\eta I_s)}{N}S - (\rho_1(t)+\mu)S\Big] \\
& + \lambda_2^*\Big[\rho_1(t)S - \frac{\tau_2 c(1-\epsilon\varphi(t))(I_a+\eta I_s)}{N}V_1 - (\omega+\rho_2(t)+\mu)V_1\Big] + \lambda_3^*\Big[\rho_2(t)V_1 - (\omega+\rho_3+\mu)V_2\Big] \\
& + \lambda_4^*\Big[\frac{\tau_1 c(1-\epsilon\varphi(t))(I_a+\eta I_s)}{N}S + \frac{\tau_2 c(1-\epsilon\varphi(t))(I_a+\eta I_s)}{N}V_1 - (\sigma+\theta+\gamma_1+\mu)L\Big] + \lambda_5^*\Big[\theta L - (\phi_1+\gamma_2+\mu)Q\Big] \\
& + \lambda_6^*\Big[\sigma(1-\psi)L - (\phi_2+\xi+\mu)I_a\Big] + \lambda_7^*\Big[\sigma\psi L + \xi I_a - (\phi_3+\delta_1+\mu)I_a\Big] + \lambda_8^*\Big[\phi_1 Q + \phi_2 I_a + \phi_3 I_s - (\gamma_3+\delta_2+\mu)P\Big] \\
& + \lambda_9^*\Big[\rho_3 V_2 + \gamma_1 L + \gamma_2 Q + \gamma_3 P - \mu R\Big],
\end{aligned} \tag{29}$$

where $\lambda_1^*, \lambda_2^*, \lambda_3^*, \lambda_4^*, \lambda_5^*, \lambda_6^*, \lambda_7^*, \lambda_8^*$ and λ_9^* are the adjoint variable by applying Pontryagin's Maximum Principle [35], we obtain the following theorem.

Theorem 6.2. *There exists an optimal control triplet $\varphi^*(t), \rho_1^*(t)$ and $\rho_2^*(t)$ and the corresponding solution, $(S^*, V_1^*, V_2^*, I_a^*, I_s^*, P^*, R^*)$ that minimizes $J\left[\epsilon, \rho_1, \rho_2\right]$ over Ω_p^0. Furthermore, there exist adjoint functions $\lambda_1^*, \lambda_2^*, \lambda_3^*, \lambda_4^*, \lambda_5^*, \lambda_6^*, \lambda_7^*, \lambda_8^*$ and λ_9^* such that*

$$
\begin{aligned}
\frac{d\lambda_1^*}{dt} &= \frac{\tau_1 c(1-\epsilon\varphi(t))(I_a^*+\eta I_s^*)}{N^*}(\lambda_1^*-\lambda_4^*)+\frac{\tau_1 c(1-\epsilon\varphi(t))(I_a^*+\eta I_s^*)S^*}{N^{*2}}(\lambda_4^*-\lambda_1^*)+\frac{\tau_1 c(1-\epsilon\varphi(t))(I_a^*+\eta I_s^*)V_1^*}{N^{*2}}(\lambda_4^*-\lambda_2^*)+\rho_1(t)(\lambda_1^*-\lambda_2^*)+\lambda_1^*\mu,\\
\frac{d\lambda_2^*}{dt} &= \frac{\tau_1 c(1-\epsilon\varphi(t))(I_a^*+\eta I_s^*)S^*}{N^{*2}}(\lambda_4^*-\lambda_1^*)+\frac{\tau_2 c(1-\epsilon\varphi(t))(I_a^*+\eta I_s^*)}{N^*}(\lambda_2^*-\lambda_4^*)+\frac{\tau_2 c(1-\epsilon\varphi(t))(I_a^*+\eta I_s^*)V_1^*}{N^{*2}}(\lambda_4^*-\lambda_2^*)\\
&\quad+\omega(\lambda_2^*-\lambda_1^*)+\rho_2(t)(\lambda_2^*-\lambda_3^*)+\lambda_2^*\mu,\\
\frac{d\lambda_3^*}{dt} &= \frac{\tau_1 c(1-\epsilon\varphi(t))(I_a^*+\eta I_s^*)S^*}{N^{*2}}(\lambda_4^*-\lambda_1^*)+\frac{\tau_2 c(1-\epsilon\varphi(t))(I_a^*+\eta I_s^*)V_1^*}{N^{*2}}(\lambda_4^*-\lambda_2^*)+\rho_3(\lambda_3^*-\lambda_9^*)+\lambda_3^*\mu,\\
\frac{d\lambda_4^*}{dt} &= \frac{\tau_1 c(1-\epsilon\varphi(t))(I_a^*+\eta I_s^*)S^*}{N^{*2}}(\lambda_4^*-\lambda_1^*)+\frac{\tau_2 c(1-\epsilon\varphi(t))(I_a^*+\eta I_s^*)V_1^*}{N^{*2}}(\lambda_4^*-\lambda_2^*),+\gamma_1(\lambda_4^*-\lambda_9^*)+\theta(\lambda_4^*-\lambda_5^*)+\sigma(\lambda_4^*-\lambda_6^*(1-\psi)-\lambda_7^*\psi)+\lambda_4^*\mu,\\
\frac{d\lambda_5^*}{dt} &= \frac{\tau_1 c(1-\epsilon\varphi(t))(I_a^*+\eta I_s^*)S^*}{N^{*2}}(\lambda_4^*-\lambda_1^*)+\frac{\tau_2 c(1-\epsilon\varphi(t))(I_a^*+\eta I_s^*)V_1^*}{N^{*2}}(\lambda_4^*-\lambda_2^*),+\gamma_2(\lambda_5^*-\lambda_9^*)+\phi_1(\lambda_5^*-\lambda_8^*)+\lambda_5^*\mu,\\
\frac{d\lambda_6^*}{dt} &= -m_1+\frac{\tau_1 c(1-\epsilon\varphi(t))S^*}{N^*}(\lambda_1^*-\lambda_4^*)+\frac{\tau_1 c(1-\epsilon\varphi(t))(I_a^*+\eta I_s^*)S^*}{N^{*2}}(\lambda_4^*-\lambda_1^*),+\frac{\tau_2 c(1-\epsilon\varphi(t))V_1^*}{N^*}(\lambda_2^*-\lambda_4^*)\\
&\quad+\frac{\tau_2 c(1-\epsilon\varphi(t))(I_a^*+\eta I_s^*)V_1^*}{N^{*2}}(\lambda_4^*-\lambda_2^*)+\xi(\lambda_6^*-\lambda_7^*)+\phi_2(\lambda_6^*-\lambda_8^*)+\lambda_6^*\mu,\\
\frac{d\lambda_7^*}{dt} &= -m_2+\frac{\tau_1 c(1-\epsilon\varphi(t))\eta S^*}{N^*}(\lambda_1^*-\lambda_4^*)+\frac{\tau_1 c(1-\epsilon\varphi(t))(I_a^*+\eta I_s^*)S^*}{N^{*2}}(\lambda_4^*-\lambda_1^*)+\frac{\tau_2 c(1-\epsilon\varphi(t))\eta V_1^*}{N^*}(\lambda_2^*-\lambda_4^*)\\
&\quad+\frac{\tau_2 c(1-\epsilon\varphi(t))(I_a^*+\eta I_s^*)V_1^*}{N^{*2}}(\lambda_4^*-\lambda_2^*)+\phi_3(\lambda_7^*-\lambda_8^*)+\lambda_7^*(\delta_1+\mu),\\
\frac{d\lambda_8^*}{dt} &= \frac{\tau_1 c(1-\epsilon\varphi(t))(I_a^*+\eta I_s^*)S^*}{N^{*2}}(\lambda_4^*-\lambda_1^*)+\frac{\tau_2 c(1-\epsilon\varphi(t))(I_a^*+\eta I_s^*)V_1^*}{N^{*2}}(\lambda_4^*-\lambda_2^*)+\gamma_3(\lambda_8^*-\lambda_9^*)+\lambda_8^*(\delta_2+\mu),\\
\frac{d\lambda_9^*}{dt} &= \frac{\tau_1 c(1-\epsilon\varphi(t))(I_a^*+\eta I_s^*)S^*}{N^{*2}}(\lambda_4^*-\lambda_1^*)+\frac{\tau_2 c(1-\epsilon\varphi(t))(I_a^*+\eta I_s^*)V_1^*}{N^{*2}}(\lambda_4^*-\lambda_2^*)+\lambda_9^*\mu,
\end{aligned}
\tag{30}
$$

with transversality conditions; $\lambda_i(t_f)=0, i=1,2,...,9$ *and* $N^*=S^*+V_1^*+V_2^*+L^*+I_a^*+I_s^*+P^*+R^*$. *The following characterization holds;*

$$
\begin{aligned}
\varphi^*(t) &= min\left[max\left(a_1,\frac{1}{m_3}\left(\frac{\tau_1 c\epsilon(I_a^*+\eta I_s^*)S^*}{N^*}(\lambda_4^*-\lambda_1^*)+\frac{\tau_2 c\epsilon(I_a^*+\eta I_s^*)V_1^*}{N^*}(\lambda_4^*-\lambda_2^*)\right),b_1\right)\right],\\
\rho_1^*(t) &= min\left[max\left(a_2,\frac{(\lambda_1^*-\lambda_2^*)S^*}{m_4}\right),b_2\right],\\
\rho_2^*(t) &= min\left[max\left(a_3,\frac{(\lambda_2^*-\lambda_3^*)V_1^*}{m_5}\right),b_3\right].
\end{aligned}
\tag{31}
$$

Proof. The proof of Theorem 6.2 is given in Appendix B. □

7. Simulations

In this section, we present the sensitivity analysis of R_{mv}, and the numerical simulations of the model (1) and the optimal control model.

7.1. Sensitivity analysis

In determining the factors responsible for the morbidity and mortality rates due to COVID-19 pandemic, it is important to carry out sensitivity analysis in order to identify the key parameters of the model necessitating the transmission and prevalence. A sensitivity of a variable with respect to model parameters is usually measured by sensitivity index. To account for this, we applied normalized forward sensitivity index as in Deressa et al. [70] on the control reproduction number as given by the equation below.

$$
S_p^{R_{mv}}=\frac{\partial R_{mv}}{\partial p}\frac{p}{R_{mv}},
\tag{32}
$$

where p represents any parameter in the model as contained in R_{ev}. For instance, the sensitivity index (S.I) of Λ is

$$
\S_\Lambda^{R_{mv}}=\frac{\partial R_{mv}}{\partial \Lambda}\frac{\Lambda}{R_{mv}}=1,
$$

and similarly for other parameters. Hence, we obtain the sensitivity indices of R_{mv} as given in Table 3 based on the parameter values in Table 2.

Note that $S_p^{R_{mv}}$ has a maximum value of 1. $S_p^{R_{mv}}=1$ implies an increase (decrease) of p by $x\%$ increases (decreases) R_{mv} by $x\%$. On the contrary, $S_p^{R_{mv}}=-1$ indicates that an increase (decrease) of p by $x\%$ decreases (increases) R_{mv} by $x\%$. The sensitivity results in Table 3 reveal that, the disease transmission and contact rates have impacts in controlling the spread of the disease as obtained in the works of [5,25]. Meanwhile, first dose vaccination rate in Table 3 has a negative correlation with the reproduction number, implying that, it can supply to the body the initial immunity needed to fight against the epidemic, as observed by [38].

7.2. Numerical simulation of model (1)

Here, we carried out different numerical experiments using the initial data relevant to COVID-19 cases in Nigeria as in Tables 1 and 2 and presented the results with discussion in the figures below. In Fig. 6, the plots show that an increase in the compliance to COVID-19 guidelines on prevention and control reduces significantly the latent and infected population, hence reducing the spread of COVID-19 as stated by [23].

Table 3
Sensitivity indices (S.I) of the parameter values.

Parameter	S.I	Parameter	S.I
Λ	1	ρ_1	−0.2849713377
ρ_2	−0.2449485467	ρ_3	$-2.152676479 \times 10^{-10}$
Ω	0.2654803270	δ_1	−0.09697582619
τ_1	0.9484008795	τ_2	0.05159912062
c	0.9999999999	ϵ	−0.8181818183
φ	−0.8181818183	ϕ_2	−0.006279000746
ϕ_3	−0.07884213514	θ	−0.02199582079
η	0.2640423100	σ	0.9430108280
γ_1	−0.9098271327	ξ	−0.6144950526

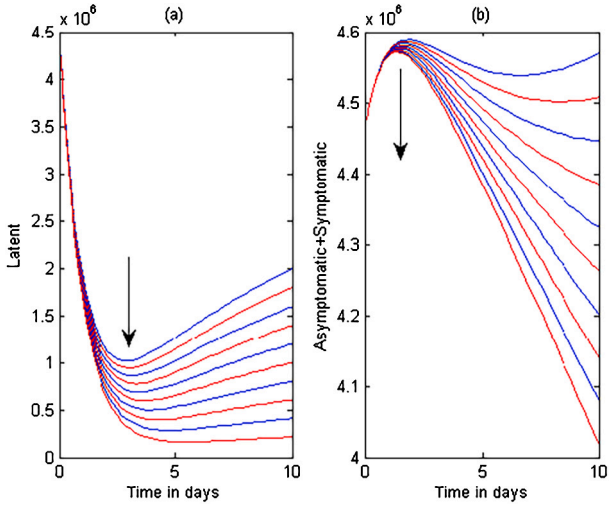

Fig. 6. Simulation of model (1) showing plots of latent and total infected (Asymptomatic and Symptomatic) individuals with media compliance (φ) increasing from 0.1 to 1 in step of 0.1 when vaccines are not in use. Apart from $c = 2$, all parameters used are from Table 2 with initial conditions in Table 1. The arrow in the figures illustrates the direction of increase in compliance.

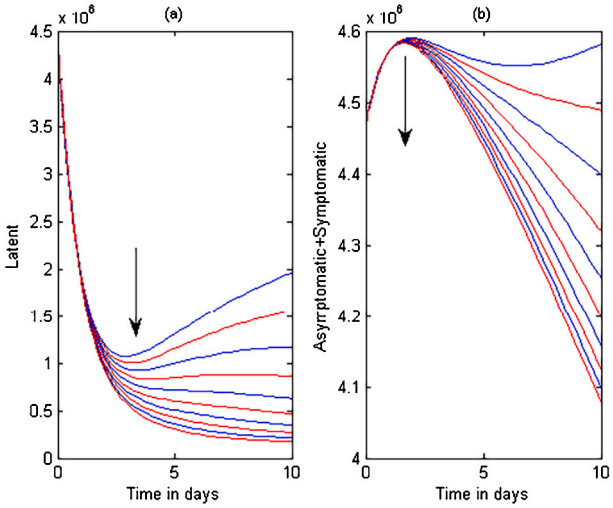

Fig. 7. Simulation of model (1) showing plots of latent and total infected (Asymptomatic and Symptomatic) individuals with vaccination doses (ρ_1, ρ_2) increasing from 0.1 to 1 in step of 0.1 when media is suspended. Apart from $c = 2$, all parameters used are from Table 2 with initial conditions in Table 1. The arrow in the figures illustrates the direction of increase in first and second doses of COVID-19 vaccine.

Fig. 7 showed that a corresponding increase in first and second doses is accompany by a corresponding decrease in the number of both the latent and infected COVID-19 cases. This is consistent with the results of the works by [38,39,41]. We observed from Figs. 6 and 7 that media has more impact on COVID-19 outbreak than vaccination since it reduces the total number of infected individuals to about 4.02×10^8 less than 4.1×10^8 achieved by double dose vaccination intervention.

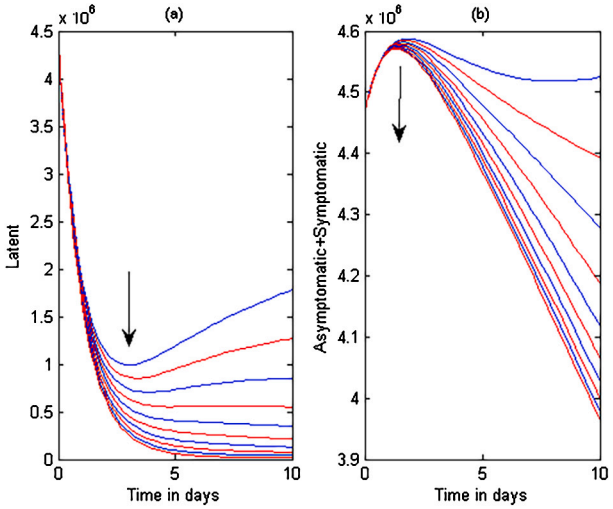

Fig. 8. Simulation of model (1) showing plots of latent and total infected (Asymptomatic and Symptomatic) individuals with media compliance and double dose vaccination $(\varphi, \rho_1, \rho_2)$ increasing from 0.1 to 1 in step of 0.1 Apart from $c = 2$, all parameters used are from Table 2 with initial conditions in Table 1. The arrow in the figures illustrates the direction of increase in compliance, first and second doses of COVID-19 vaccine.

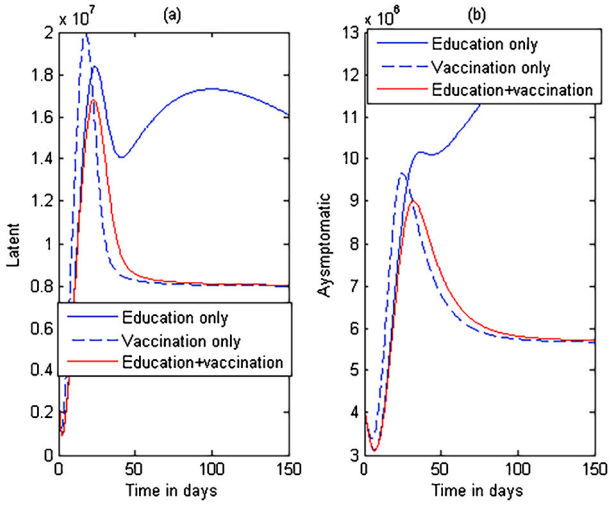

Fig. 9. Simulation of model (1) showing plots of latent and asymptomatic individuals with various interventions. Apart from $c = 2$, all parameters used are from Table 2 with initial conditions in Table 1.

Fig. 8 shows that, an increase in media compliance, first and second doses of vaccine eliminates the latently infected individuals within a week and dragged the total number of asymptomatic and symptomatic individuals to a minimal level of about 3.9×10^8 which is fewer compared to the numbers achieved by the interventions illustrated in Figs. 6 and 7. Thus, giving a better option for mitigating the spread of the pandemic. The plots in Fig. 9 show that over a long period of implementation, double dose vaccination strategy is most useful in preventing susceptible individuals from contracting COVID-19 among the latent and asymptomatic infectives since compliance to COVID-19 control guidelines seems to fade out with time. This result agrees with the report by [71] (which says, the efficiency of media campaign in disease control is constrained by time, resources and environmental factors); and the present reality in Nigeria, where most individuals are no longer adhering to COVID-19 protocols such as wearing of face masks in public places, regular washing of hands and use of alcohol-based sanitizer. Thus, continuous media campaigns with double dose vaccination should be prioritized if eradication of the pandemic is still the top agenda of the stake holders.

The next numerical results illustrates that the disease-free equilibrium is globally stable for some parameter values. In particular, Fig. 10 shows that the solution trajectories converge towards the susceptible domain of the disease-free equilibrium, $E_0 = (4.6827, 0.5404, 0.02734, 0, 0, 0, 0, 1.8079) \times 10^8$ as time approaches infinity for $R_{mv} = 0.09079 < 1$. On the other hand, the endemic equilibrium $E^* = (4.6755, 0.5396, 0.02730, 0.000277, 0.00000569, 0.00020428, 0.00000205, 1.8154) \times 10^8$ is globally stable when $R_{mv} = 1.0063 > 1$. The solution trajectories diverge away from the susceptible domain in Fig. 11.

7.3. Numerical simulation of the optimal control model

In this subsection, we discuss numerical results of model (30) to illustrate the impact of various control strategies on the spread of COVID-19 using forward-backward Runge Kutta method. We adopted initial data relevant to COVID-19 transmission dynamics in Nigeria as shown in Table 1 and the parameters in Table 2 with $\psi = 0.64, \tau_2 = 0.030$ and $c = 2$ such that $R_{mv} = 1.00063 > 1$ to generate Figs. 12-17.

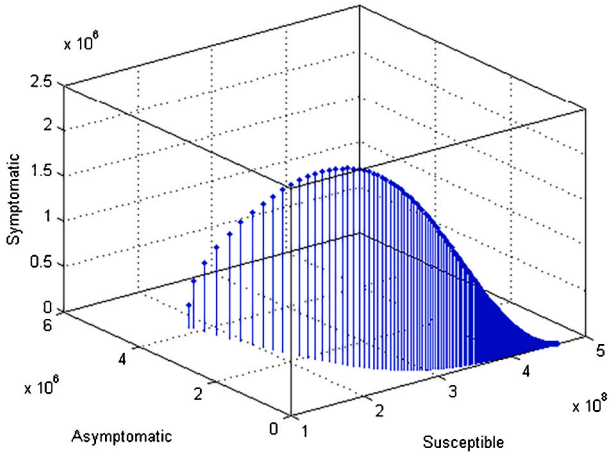

Fig. 10. Disease-free solution trajectories, $(S^0, V_1^0, V_2^0, L^0, Q^0, I_a^0, I_s^0, P^0, R^0) = (176725630, 17914944, 8197832, 4465192, 4726096, I_a(0), 255190, 2572, 249476)$. Parameter values are as in Table 2 and $I_a(0) = 100000 : 1000000 : 8000000$.

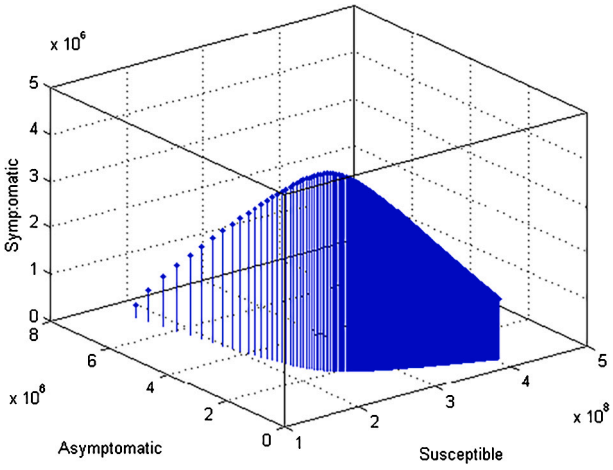

Fig. 11. Endemic solution trajectories, $(S^0, V_1^0, V_2^0, L^0, Q^0, I_a^0, I_s^0, P^0, R^0) = (176725630, 17914944, 8197832, 4465192, 4726096, I_a(0), 255190, 2572, 249476)$. Parameter values are as in Table 2 with $c = 3, \varphi = 0.64, \tau_2 = 0.030$ and $I_a(0) = 100000 : 1000000 : 8000000$.

7.3.1. Strategy one: implementing media campaign $(u_1 = \varphi)$ only

There is a significant difference in the number of latent and total infectious (asymptomatic+symptomatic) with and without control (Fig. 12). In particular, the number of latent group with and without control at the end of the period is 2.5×10^6 and 6.4×10^6, respectively, in Fig. 12a. On the other hand, the total number of infectious group is 5.3×10^6 with control and 6.4×10^6 without control in Fig. 12b. To achieve this, the control profile is implemented at maximum rate for the whole period. The control u_1 is used at its maximum level for 10 days and decreases towards zero in Fig. 12c. That means, the use of media campaign strategy for controlling COVID-19 needs maximum attention within the first days of the epidemic outbreak, as supported by the outcome in the work of [23].

7.3.2. Strategy two: administrating of first dose $(u_2 = \rho_1)$ only

The number of latent individuals at the end of the period is 2.75×10^6 and 4.4×10^6 for the cases of control and no control respectively (Fig. 13). Meanwhile, the total number of asymptomatic and symptomatic with (out) control is 5.6×10^6 (6.4×10^6) in Fig. 13b. The control profile for control u_2 is depicted in Fig. 13(c). It requires a maximum implementation through out 10 day period before declining. This indicates that, first dose vaccination is important for reducing the disease susceptibility, however, it does not support complete immunity for COVID-19 [7].

7.3.3. Strategy three: implementing media campaign and first dose of vaccination (u_1, u_2) only

Here, a pronounced difference is noticed in the total number of latent and infectious with (out) controls u_1, u_2. More precisely, the total number of latent (infectious) with controls is 1.5×10^6 (4.8×10^6) and without controls is 4.3×10^6 (6.4×10^6) (Fig. 14). It is clear that implementing u_1, u_2 optimally reduces the disease prevalence far better than u_1 or u_2 only. The control profile for the controls u_1, u_2 is shown in Fig. 14c, where both are implemented in the period of 10 days.

7.3.4. Strategy four: administrating double dose vaccination $(u_2, u_3 = \rho_2)$ only

We observed a wide difference in latent (infectious) population with and without controls. With controls u_2, u_3, the latent decreases to 1.1×10^6 and the total number of infectious individuals decline to its carrying capacity of 5.2×10^6. However, when controls are not in use, latent individuals remain 4.3×10^6 and infectious 6.4×10^6 in Fig. 15. The control profiles for u_2, u_3 are given by Fig. 15c. To achieve the above, it requires maximum of 9.9 days for u_2 and 10 days for u_3 before declining. In comparing strategies 2 and 4, it is clear from Figs. 13 and 15 that, the second dose after the first dose is necessary for eradicating the disease since strategy 4 has fewer cases of the epidemic in line with the results of [40,41].

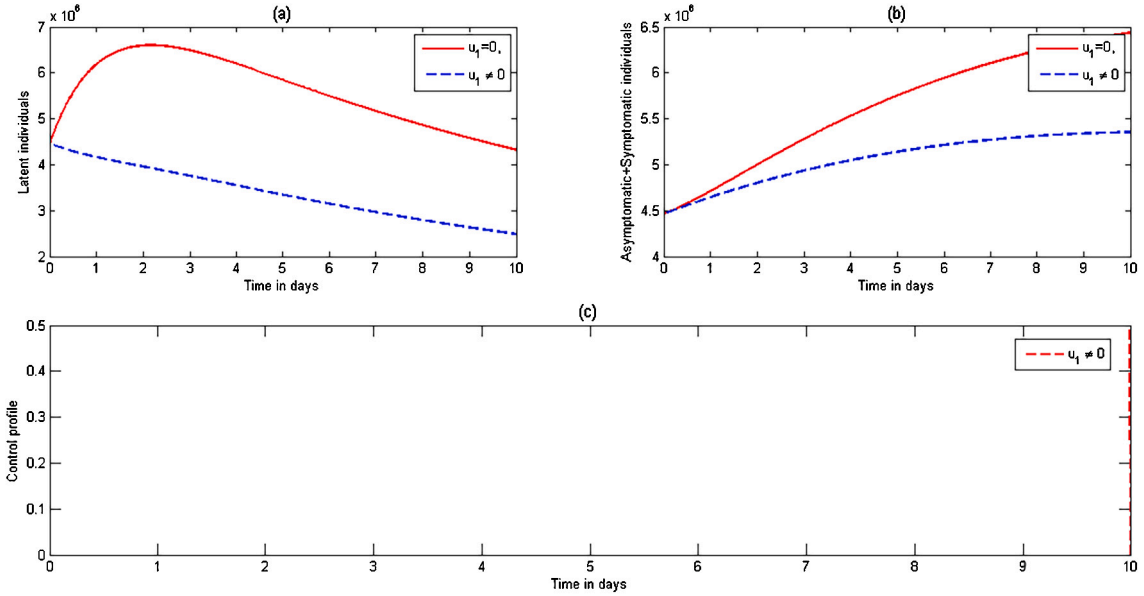

Fig. 12. Number of (a) new cases for latent individuals, (b) asymptomatic+symptomatic individuals, and (c) control profile as a function of time in the presence and absence of optimal control u_1. All parameters used are as given in Table 2.

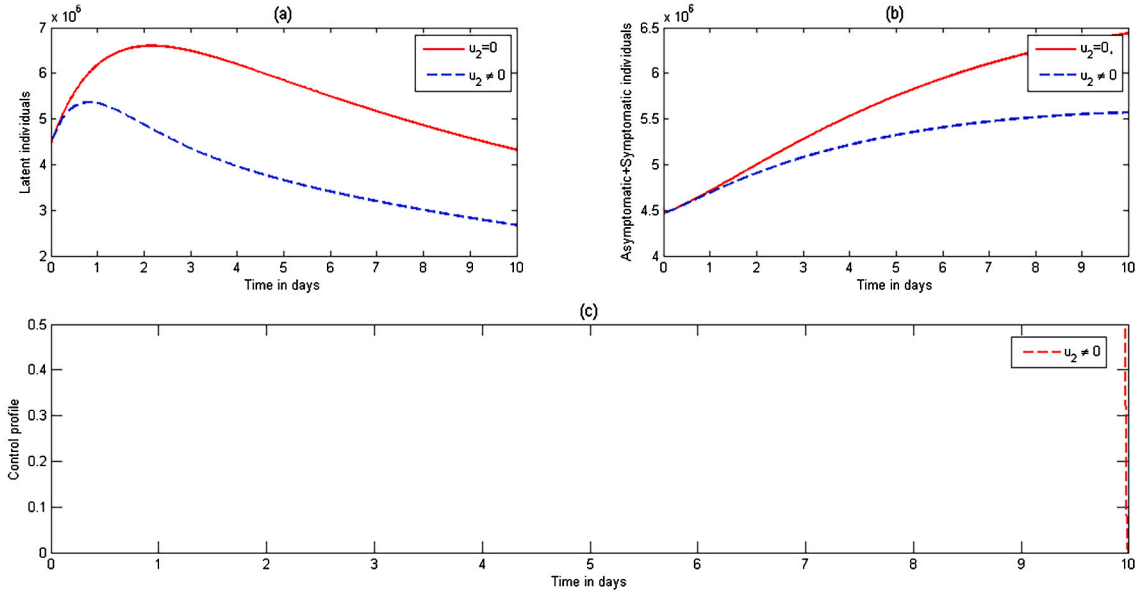

Fig. 13. Number of (a) new cases for latent individuals, (b) asymptomatic+symptomatic individuals, and (c) control profile as a function of time in the presence and absence of optimal control u_2. All parameters used are as given in Table 2.

7.3.5. Strategy five: implementing media campaign with double dose vaccination (u_1, u_2, u_3)

The application of all controls demonstrated a significant reduction in the number of latent and asymptomatic+symptomatic individuals compared to other strategies. The total number of latent (infectious) with all the controls is 0.6×10^6 (4.6×10^6) and without controls is 4.3×10^6 (6.4×10^6) at the end of the period. The control profile in Fig. 16 shows that u_1, u_2 and u_3 are to be maximized respectively in 10 days and 9.9 days before approaching to zero.

Fig. 17 shows the comparison of all the above strategies. We noticed that strategy five is the best for reducing COVID-19 burden due to latent, asymptomatic and symptomatic individuals. This is in support of the outcome of [25] which says that combined strategies are better than single controls on COVID-19 cases reduction. Inasmuch as strategy four is better than strategy three in protecting susceptible people from latent infectives, it is important to emphasis that strategy three ranks second in averting the total number of infectives. It is clear from Fig. 17 that taking first dose of COVID-19 vaccine without the second dose can not cause a break in the spreading trend of the pandemic as pointed out in the WHO's reports of 2020 [7].

8. Conclusions

In this paper, a basic mathematical model for assessing the impacts of media campaign and double dose vaccination on the dynamics of COVID-19 is formulated. The qualitative features of the model were investigated. The model has two equilibria, the disease-free equilibrium (DFE) and the

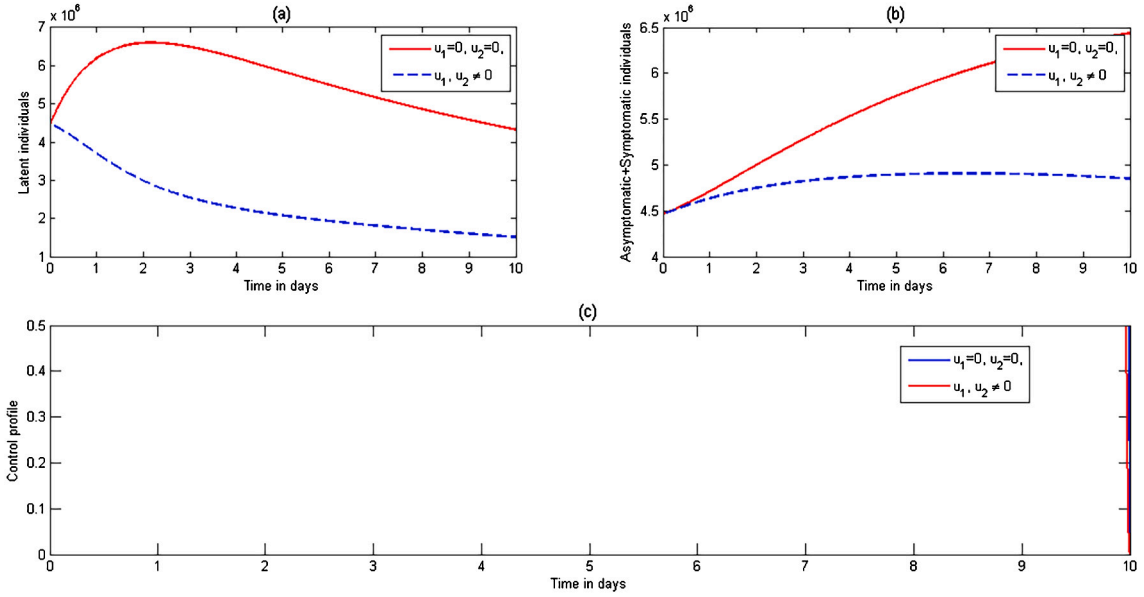

Fig. 14. Number of (a) new cases for latent individuals, (b) asymptomatic+symptomatic individuals, and (c) control profile as a function of time in the presence and absence of optimal control u_1, u_2. All parameters used are as given in Table 2.

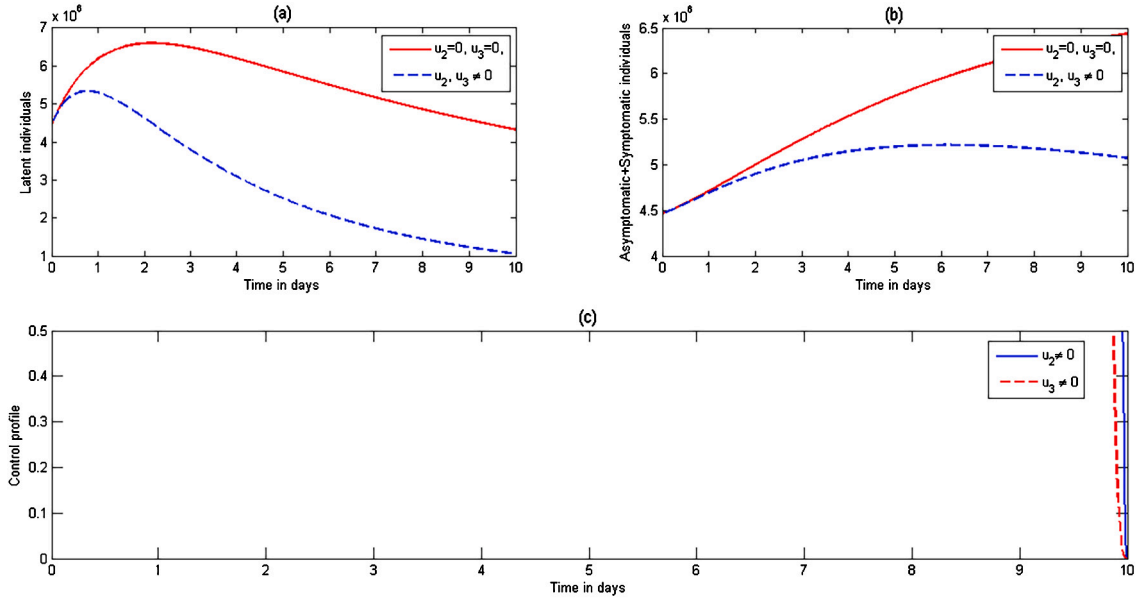

Fig. 15. Number of (a) new cases for latent individuals, (b) asymptomatic+symptomatic individuals, and (c) control profile as a function of time in the presence and absence of optimal control u_2, u_3. All parameters used are as given in Table 2.

endemic equilibrium. Theoretical results show that, the model conditionally rules out the phenomenon of backward bifurcation where a stable DFE coexists with a stable endemic equilibrium, considering the scenario by which double vaccination is suspended. Consequently, the disease-free and endemic equilibria for the model are stable (both locally and globally) when $R_{mv} < 1$ and $R_{mv} > 1$, respectively. This suggests that COVID-19 can be eradicated from the community if media campaign and double dose vaccination acquired sufficient infection blocking capacity to subject (and maintain) R_{mv} always to a value below unity. Results from sensitivity analysis showed that, a positive correlation of transmission parameters and negative one in terms of media information, first and second doses vaccine was observed with respect to the reproduction number. This implies that the rate of disease transmission needs to be controlled, probably by intense broadcasting of health information via media campaigns which promotes the benefit of additional doses of COVID-19 vaccine) otherwise a large proportion of population will be affected within a short possible time. Further, the basic model is extended to an optimal control problem with objective functional minimizer by incorporating media campaign and double dose vaccination as time dependent variables. The Pontryagin's maximum principle was employed to obtain the necessary conditions for the existence of the optimal controls that determines the eradication of the disease at a minimum cost.

Numerical simulations were obtained using some demographic data estimated from Nigeria and the remaining parameter values are assumed for the purpose of illustration. The results reported in this paper reveal that the strength of the interventions should be increased over time to eliminate the disease effectively. Mores so, to attain community herd immunity to the disease, the efficacy and compliance level of media campaign on the need to have double dose vaccination and adherence to other COVID-19 protocols, should target at least 75% coverage whenever $R_0 = 4$. Whereas when $R_0 \geq 7$, the disease can not be mitigated regardless of the level of media compliance achieved. Overall, this study shows that the prospects of

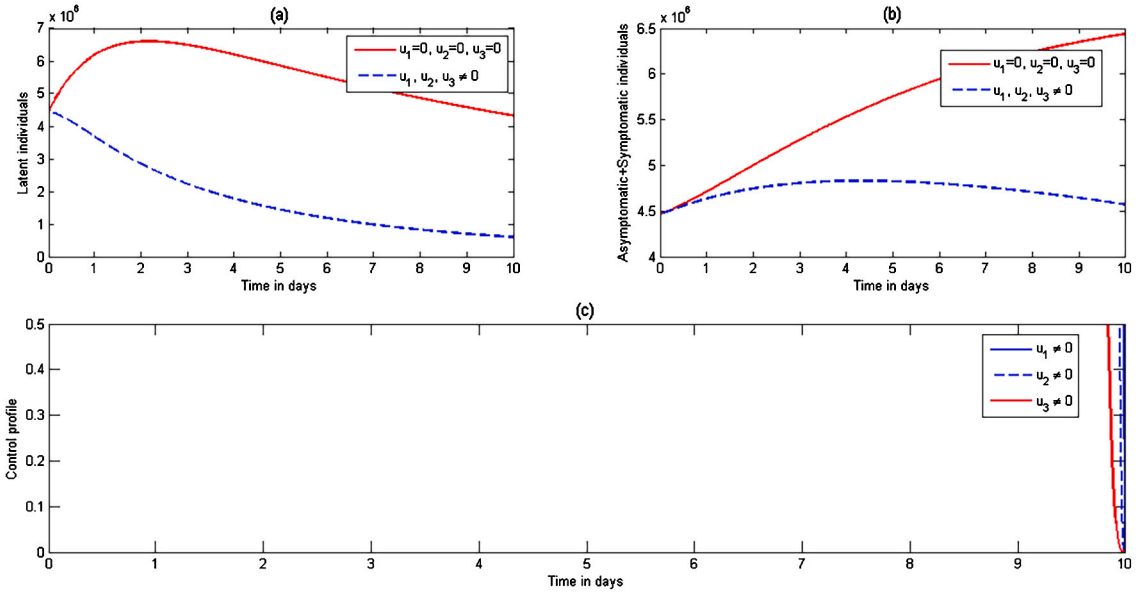

Fig. 16. Number of (a) new cases for latent individuals, (b) asymptomatic+symptomatic individuals, and (c) control profile as a function of time in the presence and absence of optimal control u_1, u_2, u_3. All parameters used are as given in Table 2.

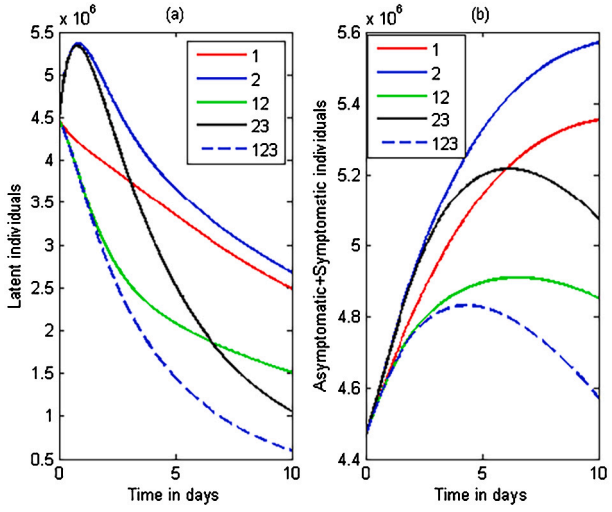

Fig. 17. Number of (a) new cases for latent individuals, and (b) asymptomatic+symptomatic individuals as a function of time showing the comparison of the above optimal control strategies. All parameters used are as given in Table 2.

effectively controlling the spread of COVID-19 in Nigeria and any other country is bright if only the optimal media campaign and double vaccination strategy can be sustained, and the time of implementation is adequately improved upon.

9. Model limitations

The following are the limitations of our model:

(i) The model caters for the long-term disease dynamics. Short-term dynamics are not considered.
(ii) The model is deterministic in nature and neither considered biological age of individuals nor the age of infection with respect to time for COVID-19 transmission. As a result, our model needs to be extended to age-structured models to cover such scenarios.
(iii) Our model did not put into consideration the impacts of media campaign and double vaccination with time delay on the transmission dynamics of the disease.
(iv) The present study is based on COVID-19 data for Nigeria only. The application of large data sets from other countries of the world can be applied to this model in subsequent studies.
(v) The epidemic peak time is fundamental for its control and eradication, therefore future works may be centred around COVID-19 peak time with respect to our model.
(vi) The fractional order form of our model (1) can be considered in subsequent studies.
(vii) Based on the analysis of the quadratic equation in (24), the possibility of backward bifurcation has been conditionally ruled out. However, for the model (1), future research works can investigate the possibility of backward bifurcation.

Declaration of competing interest

The authors declare that they have no financial or competing interests.

Acknowledgements

We wish to acknowledge the support received from the Tertiary Education Trust Fund (TETfund), Nigeria, with the award of the National Research Fund 2020 grant, reference number TETF/ES/DR&D-CE/NRF2020/SETI/82/VOL.1 to the research group which enabled us to collaborate and carry out this research work. We also appreciate our various institutions for the conducive academic environment for the pursuit of the research.

Funding

This work was supported by the Tertiary Education Trust Fund, Nigeria (TETfund) [grant number TETF/ES/DR&D-CE/NRF2020/SETI/82/VOL.1]

Appendix A. Proof of Theorem 5.4

Let $S = x_1, V_1 = x_2, V_2 = x_3, L = x_4, Q = x_5, I_a = x_6, I_s = x_7, P = x_8$ and $R = x_9$ so that $N = x_1 + x_2 + x_3 + x_4 + x_5 + x_6 + x_7 + x_8 + x_9$, hence the model (1) can be rewritten as:

$$\begin{aligned}
\dot{x_1} &= f_1 = \Lambda + \omega x_2 - \frac{\tau_1 c(1-\epsilon\phi)(x_6+\eta x_7)x_1}{x_1+x_2+x_3+x_4+x_5+x_6+x_7+x_8+x_9} - (\rho_1+\mu)x_1,\\
\dot{x_2} &= f_2 = \rho_1 x_1 - \frac{\tau_2 c(1-\epsilon\phi)(x_6+\eta x_7)x_2}{x_1+x_2+x_3+x_4+x_5+x_6+x_7+x_8+x_9} - (\omega+\rho_2+\mu)x_2,\\
\dot{x_3} &= f_3 = \rho_2 x_2 - (\rho_3+\mu)x_3,\\
\dot{x_4} &= f_4 = \frac{\tau_1 c(1-\epsilon\phi)(x_6+\eta x_7)x_1}{x_1+x_2+x_3+x_4+x_5+x_6+x_7+x_8+x_9} + \frac{\tau_2 c(1-\epsilon\phi)(x_6+\eta x_7)x_2}{x_1+x_2+x_3+x_4+x_5+x_6+x_7+x_8+x_9} - (\sigma+\theta+\gamma_1+\mu)x_4,\\
\dot{x_5} &= f_5 = \theta x_4 - (\phi_1+\gamma_2+\mu)x_5.\\
\dot{x_6} &= f_6 = \sigma(1-\psi)x_4 - (\phi_2+\xi+\mu)x_6,\\
\dot{x_7} &= f_7 = \sigma\psi x_4 + \xi x_6 - (\phi_3+\delta_1+\mu)x_7,\\
\dot{x_8} &= f_8 = \phi_1 x_5 + \phi_2 x_6 + \phi_3 x_7 - (\gamma_3+\delta_2+\mu)x_8,\\
\dot{x_9} &= f_9 = \rho_3 x_3 + \gamma_1 x_4 + \gamma_2 x_5 + \gamma_3 x_8 - \mu x_9,
\end{aligned} \tag{A.1}$$

where $f = (f_1, f_2, f_3, f_4, f_5, f_6, f_7, f_8, f_9)^T$. The Jacobian of the model (A.1) at the DFE is given by

$$J(E_0) = \begin{pmatrix}
-k_1 & \omega & 0 & 0 & 0 & \tau_1 c(1-\epsilon\varphi)B_x & \tau_1\eta c(1-\epsilon\varphi) & 0 & 0\\
\rho_1 & -k_2 & 0 & 0 & 0 & \tau_2 c(1-\epsilon\varphi)B_y & \tau_2\eta c(1-\epsilon\varphi)B_y & 0 & 0\\
0 & \rho_2 & -k_3 & 0 & 0 & 0 & 0 & 0 & 0\\
0 & 0 & 0 & -k_4 & c(1-\epsilon\varphi)F^x & \eta c(1-\epsilon\varphi)F^x & 0 & 0 & 0\\
0 & 0 & 0 & \theta & -k_5 & 0 & 0 & 0 & 0\\
0 & 0 & 0 & \sigma(1-\psi) & 0 & -k_6 & 0 & 0 & 0\\
0 & 0 & 0 & \sigma\psi & 0 & \xi & -k_7 & 0 & 0\\
0 & 0 & 0 & 0 & \phi_1 & \phi_2 & \phi_3 & -k_8 & 0\\
0 & 0 & \rho_2 & \gamma_1 & \gamma_2 & 0 & 0 & \gamma_3 & -\mu
\end{pmatrix}, \tag{A.2}$$

where $B_x = \frac{\mu k_2}{\mu(k_2+\rho_1)+\rho_1\rho_2}, B_y = \frac{\mu\rho_1}{\mu(k_2+\rho_1)+\rho_1\rho_2}, F^x = (\tau_1 B_x + \tau_2 B_y)$.

Consider the scenario when $R_{mv} = 1$. Assume that $c = c^*$ is a bifurcation parameter. Solving for c from $R_{mv} = 1$ gives $c = c^* = \frac{A}{B}$, where $A = k_4k_6k_7(\mu(k_2+\rho_1)+\rho_1\rho_2)$ and $B = (1-\epsilon\varphi)\sigma\mu\Big(k_7(1-\psi)+\eta(\xi(1-\psi)+k_6\psi)\Big)(\tau_1k_2+\tau_2\rho_1)$. Using Theorem 4.1 in [67], we can verify whether or not the model (1) has a forward bifurcation at $R_{mv} = 1$. For the scenario $R_{mv} = 1$, it can be examined that the Jacobian of matrix (13) at $c = c^*$ denoted by J_{c^*} has right eigenvectors given by $w = (w_1, w_2, ..., w_9)^T$, where

$$\begin{aligned}
w_1 &= \frac{\omega w_2 + B_1B_5w_6 + B_2B_5w_7}{k_1}, w_3 = \frac{\rho_2 w_2}{k_2}, w_5 = \frac{\theta w_4}{k_5}, w_6 = \frac{\sigma(1-\psi)w_4}{k_6},\\
w_2 &= \frac{(\rho_1B_1B_5 + k_1B_3B_6)w_6 + (\rho_1B_2B_5 + k_1B_4B_6)w_7}{k_1k_2 - \rho_1\omega}, w_7 = \frac{\sigma\psi w_4 + \xi w_6}{k_7},\\
w_8 &= \frac{\phi_1w_5 + \phi_2w_6 + \phi_3w_7}{k_8}, w_9 = \frac{\rho_2w_3 + \psi_1w_4 + \gamma_2w_5 + \gamma_3w_8}{\mu} \quad \text{and} \quad w_4 > 0 \quad \text{is a free variable.}
\end{aligned}$$

Further, J_{c^*} has a left eigenvector $v = (v_1, v_2, ..., v_9)^T$, where

$$\begin{aligned}
&v_1 = v_3 = v_5 = v_8 = v_9 = 0,\\
&v_6 = \frac{B_7v_4 + \xi v_7}{k_6}, v_7 = \frac{k_4v_4}{\sigma(1-\psi)}, \quad \text{and} \quad v_4 > 0 \quad \text{is a free variable.}
\end{aligned}$$

It follows from Theorem 4.1 in ref. [67], if we compute the non-zero partial derivatives of $\dot{x} = f(x)$ evaluated at the DFE, that the associated bifurcation coefficients a and b, defined by

$$a = \sum_{k,i,j=1}^{n} v_k w_i w_j \frac{\partial^2 f_k}{\partial x_i \partial x_j}(0,0)$$

and

$$b = \sum_{k,i=1}^{n} v_k w_i \frac{\partial^2 f_k}{\partial x_i \partial c^*}(0,0),$$

are computed to be

$$a = v_4 \frac{c^*(1-\epsilon\phi)(w_6+\eta w_7)}{N^*}\left[\tau_1(2w_1 - \frac{x_1^* B^*}{N^*}) + \tau_2(2w_2 - \frac{x_2^* B^*}{N^*})\right], \tag{A.3}$$

where $B^* = 2(w_1+w_2+w_4+w_5+w_6+w_8+w_9)+w_3(\eta+1)+w_7 > 0$ and

$$b = v_4 \frac{(1-\epsilon\phi)(w_6+\eta w_7)}{N^*}\left[\tau_1 x_1^* + \tau_2 x_2^*\right] > 0, \tag{A.4}$$

with $w_p > 0, p = 1,2,...,9$ and $v_4 > 0$. Thus, following Theorem 4.1 in [67], Theorem 5.4 is established.

Appendix B. Proof of Theorem 6.2

We apply the Pontryagin's maximum principle to have

$$\begin{aligned}
&\frac{d\lambda_1^*}{dt} = -\frac{\partial H}{\partial S}, \lambda_1^*(t_f) = 0; \frac{d\lambda_2^*}{dt} = -\frac{\partial H}{\partial V_1}, \lambda_2^*(t_f) = 0; \frac{d\lambda_3^*}{dt} = -\frac{\partial H}{\partial V_2}, \lambda_3^*(t_f) = 0;\\
&\frac{d\lambda_4^*}{dt} = -\frac{\partial H}{\partial L}, \lambda_4^*(t_f) = 0; \frac{d\lambda_5^*}{dt} = -\frac{\partial H}{\partial Q}, \lambda_5^*(t_f) = 0; \frac{d\lambda_6^*}{dt} = -\frac{\partial H}{\partial I_a}, \lambda_6^*(t_f) = 0;\\
&\frac{d\lambda_7^*}{dt} = -\frac{\partial H}{\partial I_s}, \lambda_7^*(t_f) = 0, \frac{d\lambda_8^*}{dt} = -\frac{\partial H}{\partial P}, \lambda_8^*(t_f) = 0; \frac{d\lambda_9^*}{dt} = -\frac{\partial H}{\partial R}, \lambda_9^*(t_f) = 0.
\end{aligned} \tag{B.1}$$

Considering the optimality conditions;

$$\frac{\partial H}{\varphi} = 0, \frac{\partial H}{\rho_1} = 0 \quad \text{and} \quad \frac{\partial H}{\rho_2} = 0.$$

The optimal control triplet $(\varphi^*, \rho_1^*, \rho_2^*)$ can be solved for, subject to the state variables. This yields, for the optimal control $\varphi^*(t)$,

$$\frac{\partial H}{\varphi} = m_3\varphi + \frac{\tau_1 c\epsilon(I_a+\eta I_s)S}{N}\lambda_1^* + \frac{\tau_2 c\epsilon(I_a+\eta I_s)V_1}{N}\lambda_2^* - \frac{\tau_1 c\epsilon(I_a+\eta I_s)S}{N}\lambda_4^* - \frac{\tau_2 c\epsilon(I_a+\eta I_s)V_1}{N}\lambda_4^* = 0,$$

which implies that,

$$\varphi^* = \frac{1}{m_3}\left(\frac{\tau_1 c\epsilon(I_a+\eta I_s)S}{N}(\lambda_4^* - \lambda_1^*) + \frac{\tau_2 c\epsilon(I_a+\eta I_s)V_1}{N}(\lambda_4^* - \lambda_2^*)\right)$$

For the optimal controls $\rho_1^*(t)$ and $\rho_2^*(t)$, we have

$$\begin{aligned}
&\frac{\partial H}{\rho_1} = m_4\rho_1 - S(\lambda_1^* - \lambda_2^*) = 0,\\
&\frac{\partial H}{\rho_2} = m_5\rho_2 - V_1(\lambda_2^* - \lambda_3^*) = 0,
\end{aligned}$$

which respectively gives

$$\rho_1^* = \frac{S(\lambda_1^* - \lambda_2^*)}{m_4} \quad \text{and} \quad \rho_2^* = \frac{(\lambda_2^* - \lambda_3^*)V_1}{m_5}.$$

Appendix C. Estimation of variables and parameter values

The COVID-19 data used in this work is obtained on 22nd March, 2022 from Nigeria Centre for Disease Control [3]. Total population of Nigeria, N ($N = 212,375,017$) is obtained from Worldometers [53] was used for the estimation.

E1: Natural death rate $\mu = \frac{1}{\text{life expectancy}}$, where Life expectancy in Nigeria according to Marco Trends [72] is 55.44. Thus, $\mu = \frac{1}{55.44} \approx 0.0180$.

E2: Recruitment rate $\Lambda = \mu \times N$
$\Lambda = 0.0180 \times 212,375,017 \approx 3,901,445$.

E3: Number of first dose and second dose vaccinated individuals (V_1, V_2) according to [6] are, respectively given as $(17914944, 8197832)$.

E4: Number of symptomatic cases I_s. We assumed that number of infected individuals with symbols to be the same as the total confirmed cases [3]. Thus, $I_s = 255,190$.

E5: Number of recovered individuals R. We assumed that number of recovered individuals to be the same as the Total discharged [3]. Thus, $R = 249,476$.

E6: Number of quarantined individuals Q. We assumed that number of quarantined individuals to be the same as the Total Samples tested [3]. Thus, $Q = 4,726,096$.

E7: Number of hospitalized/isolated individuals P. We assumed that number of isolated individuals to be the same as the number of Active cases [3]. Thus, $P = 2,572$.

E8: Number of Dead D. We assumed that the number of dead to be the same as the number of Total death cases [3]. Thus, $D = 3,142$.

E9: Number of Latent L

$L = \text{Total sample tested} - (\text{confirmed cases} + \text{Active cases} + \text{dead}). = 4,726,096 - (255,190 + 2,2,572 + 3,142) = 4,465,192$

E10: Number of asymptomatic individuals I_a

$I_a = \text{Latent} - (\text{symptomatic individuals}) = 4,456,196 - 255,190 = 4,210,002.$

E11: Number of susceptibles S

$S = N - (V_1 + V_2 + L + I_a + I_s + Q + P + R) = 216,746,934 - (17,914,944 + 8,197,832 + 4,210,002 + 4,465,192 + 255,190 + 4,726,096 + 2,572 + 249,476)$
$= 216,746,934 - 40,021,304 = 176,725,630.$

E12: Disease-induced death rate δ_1

$\delta_1 = \frac{\text{Total death cases}}{\text{Total confirmed cases}} = \frac{3,142}{255,190} \approx 0.0123.$

E13: Recovery rate due to treatment γ_3

$\gamma_3 = \frac{\text{Total discharged}}{\text{Total confirmed cases}} = \frac{249,476}{255,190} \approx 0.98.$

E14: Disease-induced death rate δ_2

$\delta_2 = 1 - (\mu + \gamma_3) = 1 - 0.998 = 0.002.$

E15: Quarantine rate θ

$\theta = \frac{\text{Total sample tested}}{\text{Total Nigeria population}} = \frac{4726096}{216746934} \approx 0.022.$

E16: Hospitalization rate ϕ_1

$\phi_1 = \frac{\text{Number of Active cases}}{\text{Total samples tested}} = \frac{2,572}{4,726,096} \approx 0.00054.$

E17: Hospitalization rate ϕ_2

$\phi_2 = \frac{\text{Number of Active cases}}{\text{Number of Asymptomatic individuals}} = \frac{2,572}{4,210,002} \approx 0.00061.$

E18: Hospitalization rate ϕ_3

$\phi_3 = \frac{\text{Number of Active cases}}{\text{Number of Symptomatic individuals}} = \frac{2,572}{255,190} \approx 0.01.$

E19: Progression rate σ

$\sigma = \frac{\text{Number of symptomatic casrs}}{\text{Number of latent individuals}} = \frac{255,190}{4,465,192} \approx 0.057.$

E20: Progression rate ξ

$\xi = \frac{\text{Number of symptomatic casrs}}{\text{Number of asymptomatic individuals}} = \frac{255,190}{4,210,002} \approx 0.061.$

E21: First dose vaccination rate ρ_1

$\rho_1 = \frac{\text{Number of first dose vaccinated individuals}}{\text{Total population of Nigeria}} = \frac{17,914,944}{216,746,934} \approx 0.083.$

E22: Second dose vaccination rate ρ_2

$\rho_1 = \frac{\text{Number of second dose vaccinated individuals}}{\text{Total population of Nigeria}} = \frac{8,197,832}{216,746,934} \approx 0.038.$

E23: Self immune recovery rate γ_1

$\gamma_1 = 1 - (\mu + \sigma + \theta) = 1 - (0.0180 + 0.057 + 0.022) = 0.903.$

E24: Self immune recovery rate γ_2

$\gamma_2 = \frac{\text{Total samples tested} - \text{Total confirmed cases}}{\text{Total samples tested}} = \frac{4,726,096 - 255,190}{4,726,096} \approx 0.95.$

E25: Average contact rate c

$c = \frac{\text{Number of contacts}}{\text{Total confirmed cases}} = \frac{51,038\ [54]}{255,190} \approx 0.2.$

E26: Transmission probability rate τ_1

$\tau_1 = \frac{\text{Number of unknown exposure}}{\text{Total confirmed cases}} = \frac{178,033}{255,190} \approx 0.7.$

E27: Proportion of latent ψ

$\psi = \frac{\text{Number of asymptomatic individuals, } I_a}{\text{Number of Latent, L}} = \frac{4,210,002}{4,465,192} \approx 0.94.$

E28: waning rate ω

$\omega = 1 - \text{effectiveness of first dose} = 1 - 0.33\ [54] = 0.67.$

E29: Progression rate ρ_3

$\rho_3 = \frac{\text{effectiveness of second dose } (60\% + 88\%)}{2} = \frac{148\ [7]}{2} = 74\% = 0.74.$

References

[1] WHO, WHO-weekly epidemiological updates on Covid-19, retrieved on August 14, 2022 from https://www.who.int/emergencies/diseases/novel-coronavirus-2019/situation-reports.

[2] FMOH, First case of Covid-19 confirmed in Nigeria, retrieved on August 12, 2022 from https://www.health.gov.ng.

[3] NCDC, COVID-19 Nigeria, retrieved on August 12th, 2022 from https://covid19.ncdc.gov.ng/.

[4] WHO, Coronavirus disease COVID-19 technical guidance: infection prevention and control/WASH, retrieved on August 12th, 2022 from https://www.who.int/emergies/diseases/novel-coronavirus-2019/technical-guidance/infection-prevention-and-control/.

[5] S. Khajanchi, K. Sarkar, S. Banerjee, Modelling the dynamics of Covid-19 pandemic with implementation of intervention strategies, Eur. Phys. J. Plus 137 (2022) 129, https://doi.org/10.1140/epjp/s13360-022-02347-w.

[6] NPHCDA, Nigeria hits 3.4m COVID-19 vaccination jabs in 2 rounds, retrieved on August 12th, 2022 from https://www.premiumtimesng.com/news/headlines/4750504-nigeria-hits-3.4m-covid-19-vaccine-jabs-in-2-rounds-nphda.html.

[7] WHO, Vaccine efficacy, effectiveness and protection, retrieved on August 12th, 2022 from https://www.who.int/news-room/feature-stories/vaccine-efficacy-effectiveness-and-protection.

[8] M. Turkyilmazoglu, Explicit formulae for the peak time of an epidemic from the SIR model, Physica D 422 (2021) 132902.

[9] M. Turkyilmazoglu, An extended epidemic model with vaccination: weak-immune SIRVI, Physica A 598 (2022) 127429.

[10] A. Zeb, E. Alzahrani, V.S. Erturk, G. Zaman, Analysis of cholera epidemic controlling using mathematical modelling, BioMed Res. Int. 2020 (2020) 3452402, https://doi.org/10.1155/2020/3452402.

[11] C. Maji, F.A. Basir, D. Mukherjee, K.S. Nisar, C. Ravichhandran, COVID-19 propagation and the usefulness of awarenesses control measures a mathematical model with delay, AIMS Math. 7 (7) (2022) 12091–12105.

[12] P. Samui, J. Mondal, S. Khajanchi, A mathematical model for Covid-19 transmission dynamics with a case study of India, Chaos Solitons Fractals 140 (2020) 11073.
[13] T. Sitthiwirattham, A. Zeb, S. Chasreechai, Z. Eskandari, M. Tilioua, S. Djilali, Analysis of a discrete mathematical COVID-19 model, Results Phys. 28 (2021) 104668.
[14] M.A. Alquadah, T. Abdeljawad, A. Zeb, I.U. Khan, F. Bozkurt, Effect of weather on the spread of COVID-19 using eigenspace decomposition, Comput. Mater. Continua 69 (3) (2021) 3047–3063.
[15] S. Hussain, A. Zeb, A. Rasheed, T. Saeed, Stochastic mathematical model for the spread and control of corona virus, Adv. Differ. Equ. 2020 (2020) 574, https://doi.org/10.1186/s13662-020-03029-6.
[16] Z. Zhang, A. Zeb, S. Hussain, E. Alzahran, Dynamics of COVID-19 mathematical model with stochastic perturbation, Adv. Differ. Equ. 2020 (2020) 451, https://doi.org/10.1186/s13662-020-02909-1.
[17] M.A. Alquadah, T. Abdeljawad, A. Zeb, I.U. Khan, F. Bozkurt, Deterministic and stochastic analysis of a COVID-19 spread model, Fractals 30 (5) (2022) 2240163, https://doi.org/10.1142/S0218348X22401636.
[18] Z. Zhang, A. Zeb, O.F. Egbelowo, V.S. Erturk, Dynamics of a fractional order mathematical model for COVID-19 epidemic, Adv. Differ. Equ. 2020 (2020) 420, https://doi.org/10.1186/s13662-020-02873-w.
[19] S. Bushaq, T. Saeed, D.F.M. Torres, A. Zeb, Control of COVID-19 dynamics through a fractional order model, Alex. Eng. J. 2021 (60) (2021) 5287–5296.
[20] G. Nasir, A. Zeb, K. Shah, T. Saeed, R.A. Khan, S.I.U. Khan, Study of COVID-19 mathematical model of fractional order via modified Euler method, Alex. Eng. J. 2021 (60) (2021) 3587–3592.
[21] A. Zeb, A. Atangana, Z.A. Khan, S. Djillali, A robust study of a piecewise fractional order COVID-19 mathematical model, Alex. Eng. J. 2022 (61) (2022) 5649–5665.
[22] A. Zeb, P. Kumar, V.S. Erturk, T. Sitthiwirattham, A new study on two different vaccinated fractional-order COVID-19 mathematical models via numerical algorithms, J. King Saud Univ., Sci. 34 (2022) 101914.
[23] P.K. Tiwari, K.K. Rai, S. Khajanchi, R.K. Gupta, A.K. Misra, Dynamics of coronavirus pandemic: effects of community awareness and global information campaigns, Eur. Phys. J. Plus 136 (2021) 994, https://doi.org/10.1140/epjp/s13360-021-01997-6.
[24] R.K. Rai, S. Khajanchi, P.K. Tiwari, E. Venturino, A.K. Misra, Impact of social media advertisements on the transmission dynamics of Covid-19 pandemic in India, J. Appl. Math. Comput. 68 (2020) 19–44.
[25] J. Mondal, S. Khajanchi, Mathematical modelling and optimal implementation of intervention strategies of the Covid-19 outbreak, Nonlinear Dyn. 109 (2022) 177–202, https://doi.org/10.1007/s11071-022-07235-7.
[26] S. Khajanchi, K. Sarkar, J. Mondal, K.S. Nisar, S.F. Abdelwahab, Mathematical modelling of the Covid-19 pandemic with intervention strategies, Results Phys. 25 (2021) 104285.
[27] Z.H. Shen, Y.M. Chu, M.A. Khan, S. Muhammad, O.A. Al-Hartomy, M. Higazy, Mathematical modeling and optimal control of the Covid-19 dynamics, Results Phys. 31 (2021) 105028, https://doi.org/10.1016/j.rinp.2021.105028.
[28] M.L. Diagne, H. Rwezaura, S.Y. Tchoumi, J.M. Tchuenche, A mathematical model of Covid-19 with vaccination and treatment, Comput. Math. Methods Med. 2021 (2021) 1250129, https://doi.org/10.1155/2021/1250129.
[29] M. Yavuz, F.O. Coşar, F. Gunay, F.N. Ozdemir, A new mathematical modeling of the Covid-19 pandemic including the vaccination campaign, Open J. Model. Simul. 9 (2021) 299–321.
[30] N. Nuraini, K. Sukandar, P. Hadisoemarto, H. Susanto, A. Hasan, N. Sumarti, Mathematical models for assessing vaccination scenarios in several provinces in Indonesia, Infect. Dis. Model. 6 (2021) 1236–1258.
[31] M.S. Aronna, R. Guglielmi, L.M. Moschen, A model for COVID-19 with isolation, quarantine and testing as control measures, Epidemics 34 (2021) 100437.
[32] A. Nande, B. Adlam, J. Sheen, M.Z. Levy, A.L. Hill, Dynamics of COVID-19 under social distancing measures are driven by transmission network structure, PLoS Comput. Biol. 17 (2) (2021) e1008684.
[33] O. Adedire, J.N. Ndam, Mathematical model of the spread of COVID-19 in Plateau State, Nigeria, J. Egypt. Math. Soc. 2022 (30) (2022) 10, https://doi.org/10.1186/s42787-022-00144-z.
[34] A.A. Ateneh, Y.M. Bazezew, S. Palanisamy, Mathematical model and analysis on the impact of awareness campaign and asymptomatic human immigrants in the transmission of COVID-19, BioMed Res. Int. 2022 (2022) 6260262, https://doi.org/10.1155/2022/6260262.
[35] R.I. Gweryina, C.E. Madubueze, F.S. Kaduna, Mathematical assessment of the role of denial on COVID-19 transmission with non-linear incidence and treatment functions, Sci. Afr. 12 (2021) e00811, https://doi.org/10.1016/j.sciaf.2021.e00811.
[36] S. Khajanchi, K. Sarkar, Forcasting the daily and cumulative number of cases for the Covid-19 pandemic in India, Chaos 30 (2020) 071101.
[37] K. Sarkar, S. Khajanchi, J.J. Nieto, Modelling and forecasting the Covid-19 pandemic in India, Chaos Solitons Fractals 139 (2020) 110049.
[38] A.K. Paul, M.A. Kuddus, Mathematical analysis of a Covid-19 model with double-dose vaccination in Bangladesh, Results Phys. 35 (2022) 105392.
[39] P.N.A. Akuka, B. Seidu, C.S. Bornaa, Mathematical analysis of a Covid-19 transmission dynamics model in Ghana with double-dose vaccination and quarantine, Comput. Math. Methods Med. 2022 (2022) 7493087, https://doi.org/10.1155/2022/7493087.
[40] T.A. Ayoola, M.K. Kolawole, A.O. Popoola, Mathematical model of COVID-19 transmission dynamics with double-dose vaccination, Tanzan. J. Sci. 48 (2) (2022) 499–512.
[41] O.J. Peter, H.S. Panigoro, A. Abidemi, M.M. Ojo, F.A. Oguntolu, Mathematical model of Covid-19 pandemic with double dose vaccination, Acta Biotheor. 71 (2) (2023) 9, https://doi.org/10.1007/s10441-023-09460-y.
[42] G. Sepulveda, A.J. Arenas, G. González-Parra, Mathematical modeling of Covid-19 dynamics under two vaccination doses and delay effects, Mathematics 11 (2) (2023) 369, https://doi.org/10.3390/math11020369.
[43] CDC, Possibility of COVID-19-illness after vaccination, retrieved on September 6, 2022 from https://www.cdc.gov/coronavirus/2019-ncov/vaccines/effectiveness/why-me.
[44] M. Safi, A.B. Gumel, The effect of incidences on the dynamics of quarantine/isolation model with time delay, Nonlinear Anal., Real World Appl. 12 (2011) 215–235.
[45] E. Volz, L.A. Meyers, Susceptible-infected-recovered epidemics in dynamic contact networks, Proc. R. Soc. 274 (2007) 2925–2933.
[46] J. Li, Y. Li, Y. Yang, Epidemic characteristics of two classic models and the dependence on the initial conditions, Math. Biosci. Eng. 13 (5) (2016) 999–1010.
[47] O.C. Onuegbu, J.O. Wogu, J. Agbo, The impact of social media in the fight against the spread of COVID-19 pandemic in Anambra state, Nigeria, Webology 19 (2) (2022) 6370–6388.
[48] S.A. Hong, COVID-19 vaccine communication and advocacy strategy a social marketing campaign for increasing Covid-19 uptake in South Korea pandemic in Anambra state, Nigeria, Humanit. Soc. Sci. Commun. 10 (109) (2023), https://doi.org/10.1057/s41599-023-01593-2.
[49] National Institute for Health (NIH), Lasting immunity found after recovery from Covid-19, retrieved on June 25, 2022 from https://www.nih.gov/news-events/nih-research-matters/lasting-immunity-found-after-recovery-covid-19, 2021.
[50] CDC, Quarantine and isolation, retrieved on July 7th, 2023 from https://www.cdc.gov/quarantine/index.html.
[51] World Economic Forum, COVID-19 vaccine: why it is important you get your second dose, retrieved on July 7th, 2023 from https://www.weforum.org/agenda/2021/06/covid19-vaccines-second-dose-health.
[52] S. Tan, A.T. Kwan, I. Rodriguez-Barraquet, et al., Infectiousness of SARS-COV-2 breakthrough infections and reinfections during the Omicron wave, Nat. Med. 29 (2023) 359–365.
[53] Wordometer, Nigeria population, retrieved on March 22nd, 2022 from https://www.worldometers.info/world-population/nigeria-population/.
[54] N. Akinwande, T. Ashezua, R. Gweryina, et al., Mathematical model of Covid-19 transmission dynamics incorporating booster vaccine program and environmental contamination, Heliyon 8 (11) (2022) e11513, https://doi.org/10.1016/j.heliyon.2022.e11513.
[55] D. Okuonghae, V. Aihie, Case detection and direct observation therapy strategy (dots) in Nigeria: its effect on TB dynamics, J. Biol. Syst. 16 (1) (2008) 1–31.
[56] P.V. den Driessche, J. Watmough, Reproduction numbers and sub-threshold endemic equilibria for compartmental models of disease transmission, J. Math. Biol. 180 (2002) 29–48.
[57] S. Khajanchi, S. Bera, T. Roy, Mathematical analysis of the global dynamics of a HTLV-1 infection model, considering the role of cytotoxic T-lymphocytes, Math. Comput. Simul. 180 (2021) 354–378.
[58] S. Bera, S. Khajanchi, T.K. Roy, Dynamics of an HTLV-1 infection model with delayed CTLs immune response, Appl. Math. Comput. 430 (2022) 127206, https://doi.org/10.1016/j.amc.2022.127206.
[59] N. Malunguza, S. Mushayabasa, C. Chiyaka, Z. Mukandavire, Modelling the effects of condom use and antiretroviral therapy in controlling hiv/aids among heterosexual homosexuals and bisexuals, Comput. Math. Methods Med. 11 (3) (2010) 201–222.
[60] V. Ram, L.P. Schaposnik, A modified age-structured SIR model for COVID-19 type viruses, Sci. Rep. 11 (2021) 15194, https://doi.org/10.1038/s41598-021-94609-3.
[61] K.H. Hntsa, B.N. Kahsay, Analysis of cholera epidemic controlling using mathematical modelling, Int. J. Math. Math. Sci. 2020 (2020) 7369204, https://doi.org/10.1155/2020/7369204.
[62] J.P.L. Salle, The Stability of Dynamical Systems, Hamilton Press, Berlin, New Jersey, USA, 1976.

[63] S. Cakan, Mathematical analysis of local and global dynamics of a new epidemic model, Turk. J. Math. 46 (2) (2022), https://doi.org/10.3906/mat-2107-41.
[64] H.I. Freedman, S. Ruan, M. Tang, Uniform persistence and flows near a closed positively invariant set, J. Dyn. Differ. Equ. 6 (4) (1984) 583–600.
[65] P. Samui, J. Mondal, S. Khajanchi, A mathematical model for COVID-19 transmission dynamics with a case study in India, Chaos Solitons Fractals 140 (2020) 110173.
[66] Z. Shuai, P. van den Driessche, Global stability of infectious disease models using Lyapunov functions, SIAM J. Appl. Math. 73 (4) (2013) 1513–1532.
[67] C. Castillo-Chavez, B. Song, Dynamical models of tuberculosis and their applications, Math. Biosci. Eng. 1 (2) (2004) 361–404.
[68] M.S. Goudiaby, L.D. Gning, M.L. Diagne, B.N. Dia, H. Rwezaura, J.M. Tchuenche, Optimal control analysis of a COVID-19 and tuberculosis co-dynamics model, Inf. Med. Unlock. 28 (2022) 100849, https://doi.org/10.1016/j.imu.2022.100849.
[69] R.I. Gweryina, C.E. Madubueze, V.P. Bajiya, F.E. Esla, Modelling and analysis of tuberculosis and pneumonia coinfection dynamics with cost-effectiveness, Res. Control Opt. 10 (2023) 10020.
[70] C.T. Deressa, Y.O. Mussa, G.F. Duressa, Optimal control and sensitivity analysis for transmission dynamics of coronavirus, Results Phys. 19 (2020) 103642.
[71] X. Zhao, Health communication campaigns: a brief introduction and call for dialogue, Int. J. Nurs. Sci. 7 (2020) S11–S15.
[72] Macro Trends, Nigeria life expectancy 1950-2022, retrieved on September 22nd, 2022 from https://www.macrotrends.net/countries/NGA/nigeria/life-expectancy.